JGR Oceans

RESEARCH ARTICLE
10.1029/2019JC015552

Twenty-Year Variations in Satellite-Derived Chlorophyll-a and Phytoplankton Size in the Bohai Sea and Yellow Sea

Xuerong Sun[1], Fang Shen[1,2], Robert J.W. Brewin[3,4], Dongyan Liu[1], and Rugang Tang[1]

[1]State Key Laboratory of Estuarine and Coastal Research, East China Normal University, Shanghai, China, [2]Institute of Eco-Chongming (IEC), East China Normal University, Shanghai, China, [3]College of Life and Environmental Sciences, University of Exeter, Penryn Campus, UK, [4]Plymouth Marine Laboratory, Plymouth, UK

Key Points:
- The SST-dependent three-component model was retuned and validated for remotely sensed PSCs in the Bohai Sea and Yellow Sea
- Monthly variations of PSCs derived from 20-year time series satellite data were correlated with physical variables in the central Yellow Sea
- Different impacts of each type of El Niño events in climate variability on interannual variations of PSCs were observed and related to SST

Correspondence to:
F. Shen,
fshen@sklec.ecnu.edu.cn

Citation:
Sun, X., Shen, F., Brewin, R. J. W., Liu, D., & Tang, R. (2019). Twenty-Year Variations in Satellite-Derived Chlorophyll-a and Phytoplankton Size in the Bohai Sea and Yellow Sea. *Journal of Geophysical Research: Oceans*, *124*. https://doi.org/10.1029/2019JC015552

Received 9 AUG 2019
Accepted 14 NOV 2019
Accepted article online 18 NOV 2019

Abstract Phytoplankton cell size is a useful ecological indicator for evaluating the response of phytoplankton community structure to environmental changes. Ocean-color remote observations and algorithms have allowed us to estimate phytoplankton size classes (PSCs) at decadal scale, helping us to understand their trends under ocean warming. Here a large data set of pigments, derived through high performance liquid chromatography, was collected in the Bohai Sea (BS) and Yellow Sea (YS) between 2014 and 2016. The data set was used to reparametrize the sea surface temperature (SST)-dependent three-component model of Brewin et al. (2017) to the region. The model was validated using independent in situ data set and subsequently applied to satellite chlorophyll-a data from Ocean Colour Climate Change Initiative, spanning from 1997 to 2016, to derive percentages of three PSCs to total chlorophyll-a. Monthly-averaged PSCs exhibited spatial-temporal variations in the study area, linked to topography, temperature, solar radiation, currents, and monsoonal winds. In the surface central south Yellow Sea (SYS), influenced by bottom Yellow Sea Cold Water Mass, tight relationships between PSCs and environmental factors were observed, where high SST, high sea level anomaly, low mixed-layer depth, and low wind speed resulted in higher proportions of nanoplankton and picoplankton from June to October. Significant interannual anomlies in PSCs were found associated with El Niño events in the central SYS, related to anomalies in SST. The refined model characterized 20-year variations in chlorophyll-a concentration and PSCs in complicated optical, hydrodynamic, and biogeochemical environments in the BS and YS.

Plain Language Summary Phytoplankton are the fundamental component of the marine ecosystem, and the size structure of phytoplankton influences many processes in phytoplankton biology, marine ecology, and marine biogeochemistry. Phytoplankton can be divided into three phytoplankton size classes (PSCs): microplankton (>20 μm), nanoplankton (2–20 μm), and picoplankton (<2 μm). The Bohai Sea (BS) and Yellow Sea (YS) are shallow marginal seas in the northwest Pacific Ocean, strongly impacted by large river plumes, ocean processes, and seasonal monsoons, supporting high primary and fishery productivity. Using a 20-year time series satellite ocean color data from 1997 to 2016, and a SST-dependent model that links chlorophyll-a concentration to the size structure of phytoplankton, we observe spatial and temporal variations of PSCs in the BS and YS and tight correlations between the size structure and physical variables in the central south Yellow Sea. Interannual variations in the PSCs are coupled with changes of sea surface temperature in El Niño events. Our results demonstrate that variations in the phytoplankton size structure are coupled with changes in climate variability, with implications for how the regional ecosystem may change with predicted changes in climate.

1. Introduction

Phytoplankton play an important role in global net primary production and in the marine carbon cycle (Field et al., 1998; Longhurst et al., 1995). Over past few decades, in situ measurements of phytoplankton have been collected extensively and globally. Meanwhile, since the end of last century, we have witnessed a rapid development in ocean-color remote sensing that has revolutionized our understanding of phytoplankton through continuous and synoptic data on chlorophyll-a concentration, as an index of phytoplankton biomass (Behrenfeld et al., 2006; Gregg & Conkright, 2002; Liu & Wang, 2013; McClain, 2009). However, chlorophyll-a concentration does not provide a full description of the community and function of phytoplankton. Phytoplankton have high diversity and are composed of various taxonomical

groups which contribute to a wide range of biological and biogeochemical functions (IOCCG, 2014; Nair et al., 2008; Reynolds et al., 2002). Phytoplankton cell size is considered to be a critical trait that influences metabolic rates, light absorption, nutrient uptake, carbon cycle, and the marine food web (Ciotti et al., 2002; Finkel et al., 2009; Guidi et al., 2009; Ward et al., 2012). Partitioning phytoplankton into the three size classes of microplankton (>20 μm), nanoplankton (2–20 μm), and picoplankton (<2 μm), following the classification of Sieburth et al. (1978), has been adopted widely as a simple method of quantifying phytoplankton community structure. In recent years, approaches have been presented to map PSCs at synoptic scales using satellite observations of ocean color (Brewin et al., 2017; IOCCG, 2014; Mouw et al., 2017). These approaches include spectral-based, abundance-based, and ecological-based methods (Brewin et al., 2011). Spectral-based approaches use the optical signatures of phytoplankton absorption and backscattering directly for detection (Ciotti et al., 2002; Ciotti & Bricaud, 2006; Kostadinov et al., 2009; Uitz et al., 2008). Abundance-based approaches use covariations between PSCs and an index of phytoplankton abundance or biomass, such as the total chlorophyll-a concentration, which can be retrieved with reasonable accuracy from space (Brewin et al., 2010; Devred et al., 2006; Hirata et al., 2011; Uitz et al., 2006). Ecological-based approaches use, in addition to ocean-color data, information about the environment (e.g., irradiance, SST) for classification, which can also be obtained from satellites (Brewin et al., 2017, 2015; Raitsos et al., 2008; Ward, 2015). Each approach has its own advantages and limitations (Mouw et al., 2017). Many of these approaches have been designed for global ocean applications (Brewin et al., 2015; Bricaud et al., 2012), and some regional studies have also been conducted (Brotas et al., 2013; Lamont et al., 2018; Sun et al., 2017, 2018).

The YS is a semienclosed shallow marginal sea in the northwest Pacific Ocean, connecting with the BS through the Bohai Strait (Figure 1). The topography varies from shallow coastal continental shelf waters to a deep north-southeast narrow trough in the center. Among the many rivers from the Chinese and Korean continents, two large rivers (i.e., Yellow River and Changjiang River) flow into the BS and YS, characterized by high turbidity and productivity. Under the influence of topography and seasonal variations in the East Asian monsoon and associated hydrodynamics, a noticeably large area of cold water mass, bordered by a 10 °C isotherm in the trough is found in the bottom water during the summer half year, which is called the Yellow Sea Cold Water Mass (YSCWM). For decades, numerous studies have focused on the formation mechanisms and physical dynamics of the YSCWM (Feng et al., 1992; He et al., 1959; Oh et al., 2013; Park et al., 2011; Yu et al., 2006; Zhang et al., 2008; Zhu et al., 2018), and have highlighted vertical variations in nutrients and oxygen (Wang et al., 2014; Wei, Yu, et al., 2016; Xin et al., 2015) and consequently in biological communities over the water column (Bai et al., 2007; Fu et al., 2016; Liu et al., 2015, 2012). The impact that the YSCWM has on PSCs has been mostly studied through in situ data collection and analysis (Fu et al., 2010, 2009). However, impacts of environmental factors on monthly and interannual variations of PSCs using satellite data are fairly limited.

The purpose of this study is to use a long time series satellite-based products to describe spatial-temporal vaiations of chlorophyll-a concentration and PSCs in the BS and YS. Specially, due to the exsitense of YSCWM in the summer half year, we aim to investigate the impacts of physical variables on the monthly and interannual variations of size composition in the surface central SYS. The SST-dependent three-component model (Brewin et al., 2017) was reparametrized and validated, for the first time, for estimating PSCs in the highly productive BS and YS, using in situ measurements and an independent data set of satellite and in situ matchups. Remotely sensed distributions of monthly chlorophyll-a concentration and size structure were produced in the region for the last 20 years. Spatial and temporal variations of PSCs were investigated in relation to major controlling environmental factors in the surface waters of the YSCWM in the central SYS. Interannual variations in PSCs and environmental factors were calculated, and implications of the different types of El Niño events for PSCs were investigated.

2. Data and Methods

2.1. In Situ Data

A total of 284 surface phytoplankton pigment data derived from high performance liquid chromatography (HPLC) were obtained in the BS and the YS (Figure 1). To avoid the influence of unusual blooms of high chlorophyll-a concentration on tuning the three-component algorithm, 22 samples with

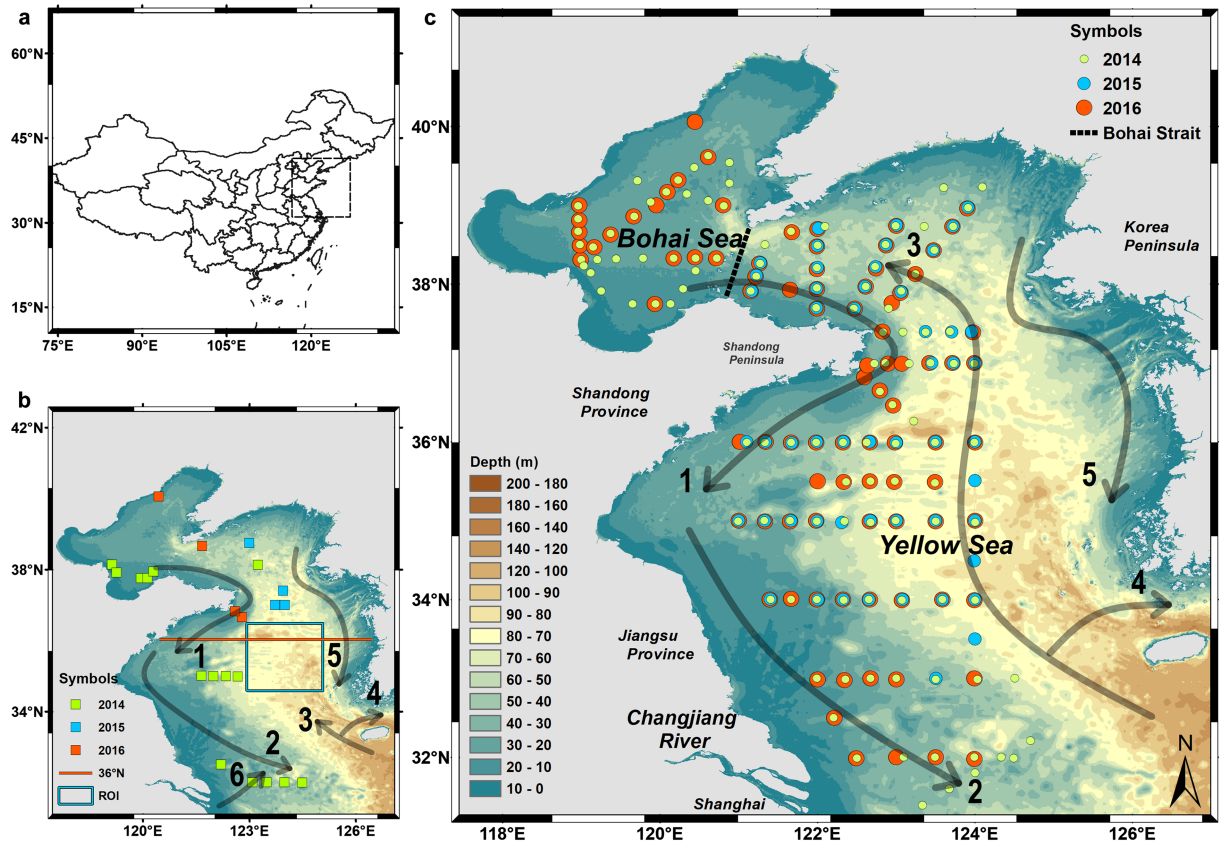

Figure 1. (a) Location of the study area. (b) Locations of independent matchups ($N = 23$) between in situ and satellite data in 2014, 2015, and 2016. The black arrows represent the water currents in the summer half year. The 36°N transect and the region of interest (ROI) related to Yellow Sea Cold Water Mass used in the analyses of monthly variation. (c) Locations of in situ reparametrization data set ($N = 239$) in 2014, 2015, and 2016. The black arrows represent the water currents in winter half year. The approximate locations of currents were based on Chen (2009) and Li et al. (2016). Number 1, Shandong Peninsula Coastal Current; 2, Yellow Sea Coastal Current; 3, Yellow Sea Warm Current; 4, Cheju Warm Current; 5, Korea Coastal Current; and 6, Changjiang Diluted Water. Note that the Changjiang Diluted Water out of the Changjiang estuary flow southwards in the winter half year, which is not shown in Figure 1c. The background seawater depth (The GEBCO_2014 Grid, version 20150318) was obtained from GEBCO (http://www.gebco.net/).

chlorophyll-a concentration higher than 5.00 mg/m^3 were removed, leaving a total of 262 samples for analysis, including 120 samples in 2014 (28 April to 18 May), 52 samples in 2015 (17 to 31 August), and 90 samples in 2016 (29 June to 15 July). The 23 of 262 samples (details in section 2.2.1) were removed to be used for independent satellite validation, leaving 239 samples for model reparametrization.

Surface water samples were collected using Niskin bottles attached to the conductivity-temperature-depth profiler (Seabird 911) rosette. For HPLC pigment concentration, water samples (500–2,000 ml) were filtered to Whatman GF/F Glass Microfiber Filters (pore size 0.7 μm, diameter 25 mm), and filters were stored in the aluminum foil and frozen in liquid nitrogen. Pigments data were measured and processed using the method of Zhang et al. (2016) in 2014 and 2015 and of Wang et al. (2016) in 2016. Chlorophyll-a and seven diagnostic pigments concentrations (i.e., fucoxanthin, peridinin, 19-hex-fucoxanthin, alloxanthin, 19-but-fucoxanthin, chlorophyll-b, and zeaxanthin) were quantified. Size-fractionated concentrations and percentages were calculated using diagnostic pigment analysis (Brewin et al., 2010; Hirata et al., 2011; Uitz et al., 2006; Vidussi et al., 2001) with some adjustments according to the study area, where chlorophyll-b was regarded as a biomarker of nanoplankton, as explained in Sun et al. (2018). Fractions of each PSCs to total chlorophyll-a concentration can be inferred as

$$C_E = \sum_{i=1}^{7} W_i P_i, \tag{1}$$

$$F_m = \frac{\sum_{i=1}^{2} W_i P_i}{C_E}, \tag{2}$$

$$F_{\mathrm{n}} = \begin{cases} \dfrac{12.5 C_{HPLC} W_3 P_3 + \sum_{i=4}^{6} W_i P_i}{C_E} & , C_{HPLC} < 0.08 mg/m^3 \\ \dfrac{\sum_{i=3}^{6} W_i P_i}{C_E} & , C_{HPLC} > 0.08 mg/m^3 \end{cases}, \tag{3}$$

$$F_p = \begin{cases} \dfrac{(-12.5 C_{HPLC} + 1) W_3 P_3 + W_7 P_7}{C_E} & , C_{HPLC} < 0.08 mg/m^3 \\ \dfrac{W_7 P_7}{C_E} & , C_{HPLC} > 0.08 mg/m^3 \end{cases}, \tag{4}$$

where, $[W] = \{1.41; 1.41; 1.27; 0.6; 0.35; 1.01; 0.86\}$ and $[P] = \{$fucoxanthin; peridinin; 19-hex-fucoxanthin; alloxanthin; 19-but-fucoxanthin; chlorophyll-b; zeaxanthin$\}$. The subscripts m, n, and p refer to microplankton (>20 μm), nanoplankton (2–20 μm), and picoplankton (<2 μm), respectively. C_E and C_{HPLC} represent estimated chlorophyll-a concentration from seven diagnostic pigment data and measured chlorophyll-a concentration from HPLC.

2.2. Satellite Data

2.2.1. Chlorophyll-a Concentration and Remote Sensing Reflectance Data

The merged SeaWiFS, MERIS, Aqua-MODIS, and VIIRS chlorophyll-a concentration and remote sensing reflectance (R_{rs}) data with a resolution of 4 km from version 3.1 of the Ocean Colour Climate Change Initiative (OC-CCI, https://www.oceancolour.org/) were used in this study, including daily and monthly composites. The chlorophyll-a concentration products are generated using a blended combination of algorithms of OCI (OC4V6+CI), OC3, and OC5, weighted by specific water classes, which improves performance in Case-2 waters (i.e., accounting for substances other than phytoplankton that have an effect on the ocean-color signal). The R_{rs} values from MERIS, MODIS, and VIIRS are band-shifted to standard SeaWiFS wavelengths (i.e., 412, 443, 490, 510, 555, and 670 nm).

The quality assurance (QA) scores (Wei, Lee, & Shang , 2016) were calculated to evaluate the data quality of the merged OC-CCI R_{rs} data (MATLAB R2014b, available at http://oceanoptics.umb.edu/score_metric/). The QA score system was adapted for six wavelengths of OC-CCI R_{rs} data (i.e., 412, 443, 490, 510, 555, and 670 nm), resulting in quality scores varying from 0 (lowest quality) to 1 (highest quality). To ensure the quality of satellite chlorophyll-a products during validation, questionable R_{rs} data were excluded, and 23 matchups are retained only when the QA score is 1. In situ chlorophyll-a measurements were matched to daily OC-CCI chlorophyll-a products with a 3-by-3 pixel box in 2014, 2015, and 2016. A total of 232 monthly merged OC-CCI chlorophyll-a images from September 1997 to December 2016 were used as input to derive monthly averaged PSCs. Monthly OC-CCI chlorophyll-a products with a 3-by-3 pixel box were used to analyze variations in the 36°N transect.

2.2.2. Sea Surface Temperature Data

Daily (1/4° resolution) and monthly (1° resolution) composites of Optimal Interpolation Sea Surface Temperature (OISST, version 2) data were downloaded from the NOAA website (https://www.esrl.noaa.gov/psd/data/gridded/tables/sst.html). Each daily and monthly composite was reprojected to 4-km resolution in order to match OC-CCI chlorophyll-a concentration data. In situ SST measurements were matched to daily OISST products with a 3-by-3 pixel box for 23 matchups, with the correlation coefficient $r = 0.971$ and p value < 0.001. Monthly OISST data were obtained for the same time period (from October 1997 to December 2017) for deriving PSCs.

2.2.3. Other Environmental Variables

Based on the SL-TAC multimission altimeter data (i.e., Jason-3, Sentinel-3A, HY-2A, Saral/AltiKa, Cryosat-2, Jason-2, Jason-1, T/P, ENVISAT, GFO, ERS1/2) processing system, daily mean sea level anomaly (SLA) data (1/4° resolution) computed with respect to a 20-year mean were downloaded from Copernicus Marine Environment Monitoring Service (http://marine.copernicus.eu/). Monthly SLA data were produced from averaging daily data.

Monthly mixed-layer depth (MLD) data (1/12° resolution) were obtained from Copernicus Marine Environment Monitoring Service (http://marine.copernicus.eu/). The MLD was defined as the depth where density increase compared to density at 10-m depth corresponds to temperature decrease of 0.2 °C in local surface conditions.

The Cross-Calibrated Multi-Platform (CCMP) version 2.0 gridded surface vector winds data are produced based on satellite, moored buoy, and model winds data, including two arrays of wind components at 1/4° resolution, acquiring from the Remote Sensing Systems website (http://www.remss.com/measurements/ccmp/). Winds in the CCMP products are of oceanographic convection, meaning the positive UWind and VWind is to the right and above the axis, respectively.

The SLA, MLD, and CCMP vector winds data were reprojected to 4-km resolution via bilinear interpolation through the software SeaDAS (version, 7.5.1), based on the spatial information of OC-CCI chlorophyll-a data, for the same period from September 1997 to December 2016.

2.2.4. Climate Indices

The Oceanic Niño Index (ONI), defined as the three month running-mean SST departures in the Niño 3.4 region (5°N-5°S, 120°W-170°W), was downloaded from the website of NOAA Climate Prediction Center (https://origin.cpc.ncep.noaa.gov/), where El Niño is characterized by a positive ONI greater than or equal to 0.5 °C. Based on the location of maximum SST anomalies, El Niño events are classified into two types, referred to as the Eastern Pacific (EP) and Central Pacific (CP) El Niño (Kao & Yu, 2009; Takahashi et al., 2011). Time series of monthly EP and CP El Niño indices were downloaded from https://www.ess.uci.edu/~yu/2OSC/. The EP index is calculated by first removing SST anomalies which are regressed with Niño4 index (i.e., representing the influence of central Pacific warming), and then using empirical orthogonal function analysis to characterize spatial patterns of EP El Niño events. Similarly, the CP index is calculated by removing SST anomalies, which are regressed with Niño1+2 index (i.e., representing the influence of eastern Pacific warming), and then using empirical orthogonal function analysis to determine spatial patterns of CP El Niño events (Kao & Yu, 2009). The period 1997–2016 includes one strong EP El Niño event in 1997–1998, three CP El Niño events in 2002–2003, 2004–2005, and 2009–2010, and two mixed El Niño events in 2006–2007 and 2015–2016 (Paek et al., 2017; Yu & Kim, 2013).

2.3. Estimation of Phytoplankton Size Classes

2.3.1. The Modification of Three-Component Model with SST

Based on two exponential functions (Sathyendranath et al., 2001), the three-component model of Brewin et al. (2010, 2015) was developed for estimating PSCs as a function of total chlorophyll-a concentration, according to

$$P_{n,p} = \frac{C_{n,p}^{m}\left[1-\exp\left(-\frac{D_{n,p}}{C_{n,p}^{m}} * C_{HPLC}\right)\right]}{C_{HPLC}} * 100, \tag{5}$$

and

$$P_{p} = \frac{C_{p}^{m}\left[1-\exp\left(-\frac{D_{p}}{C_{p}^{m}} * C_{HPLC}\right)\right]}{C_{HPLC}} * 100, \tag{6}$$

where, $P_{n,p}$ and P_p are percentages of total chlorophyll-a for combined nanoplankton and picoplankton (<20 μm) and picoplankton (<2 μm). The parameters *We couldn't revise this paramter into a correct way.Please find the equation (5) for the correct one.The "m" is superscript, the "n, p" is subscript, the "m" is above the "n, p".Cm n, p* and *Please find the equation (6) for the correct one.The "m" is superscript, the "p" is subscript, the "m" is above*

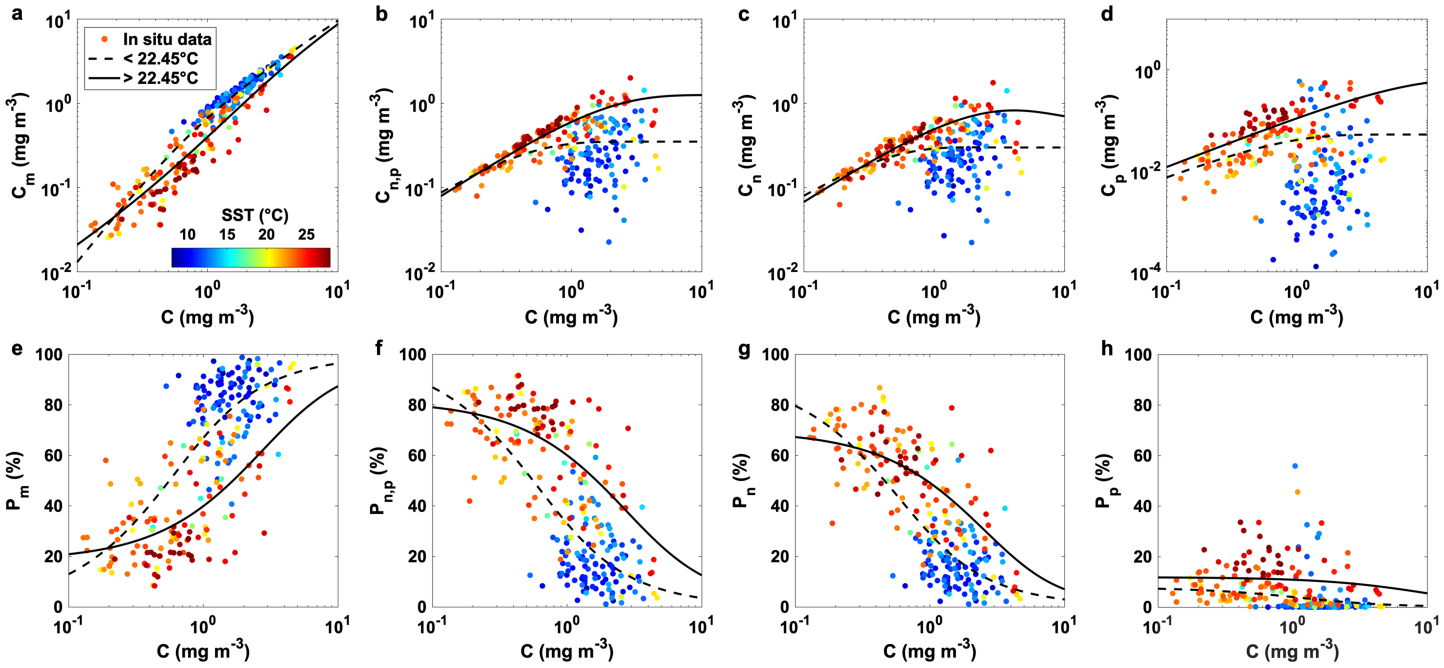

Figure 2. Relationships between size-fractionated concentration (a, b, c, d) and percentages (e, f, g, h), as a function of total chlorophyll-a concentration with the color representing SST. Dotted lines and solid lines represent estimates derived from three-component model using model parameters for low and high SST waters, respectively.

the "p".Cm p are the asymptotic maximum values (units in mg/m^3) for the two size classes, and $D_{n,p}$ and D_p represent the fraction of two size classes as total chlorophyll-a concentration tends to zero. Since size-fractionated chlorophyll-a concentration will never exceed total concentration, $D_{n,p}$ and D_p are forced to less than or equal to 1. C_{HPLC} represents measured chlorophyll-a concentration from HPLC.

Significant relationships between SST and model parameters (*Please find the equation (5) for the correct one. The "m" is superscript, the "n, p" is subscript, the "m" is above the "n, p".Cm n,p*, *Please find the equation (6) for the correct one.The "m" is superscript, the "p" is subscript, the "m" is above the "p".Cm p,* $D_{n,p}$, and D_p) have been observed in the northeast Atlantic. Brewin et al. (2017) related the parameters of the model to SST, according to,

$$C_{n,p}^{m} = 1 - \left\{ \frac{G_1}{1 + \exp[-G_2(\mathrm{SST} - G_3)]} + G_4 \right\}, \tag{7}$$

$$C_{p}^{m} = 1 - \left\{ \frac{H_1}{1 + \exp[-H_2(\mathrm{SST} - H_3)]} + H_4 \right\}, \tag{8}$$

$$D_{n,p} = \frac{J_1}{1 + \exp[-J_2(\mathrm{SST} - J_3)]} + J_4, \tag{9}$$

and

$$D_{p} = \frac{K_1}{1 + \exp[-K_2(\mathrm{SST} - K_3)]} + K_4, \tag{10}$$

where, G_1 and G_4 control the upper and lower bounds of *Please find the equation (5) for the correct one.The "m" is superscript, the "n, p" is subscript, the "m" is above the "n, p".Cm n,p*, G_2 is the slope of change in *Please find the equation (5) for the correct one.The "m" is superscript, the "n, p" is subscript, the "m" is above the "n, p". Cm n,p* with SST, and G_3 represents the SST midpoint of the slope between *Please find the equation (5) for the correct one.The "m" is superscript, the "n, p" is subscript, the "m" is above the "n, p".Cm n,p* and SST. For H_i, J_i and K_i where i = 1–4 for *Please find the equation (6) for the correct one.The "m" is superscript, the "p" is*

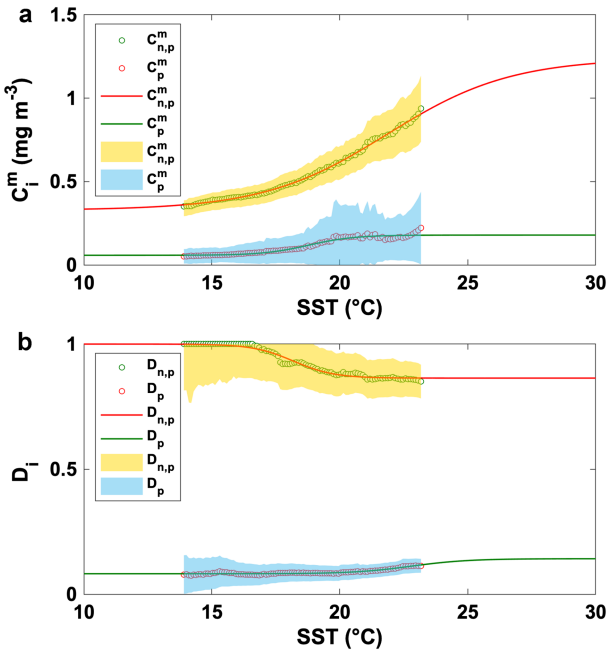

Figure 3. Relationships between SST and parameters of three-component model, (a) *Please find the equation (5) for the correct one.The "m" is superscript, the "n, p" is subscript, the "m" is above the "n, p".Cm n,p* and *Please find the equation (6) for the correct one.The "m" is superscript, the "p" is subscript, the "m" is above the "p".Cm p*, and (b) $D_{n,p}$ and D_p. Green circles represent combination of nanoplankton and picoplankton while red ones for picoplankton. Red and green lines show estimates obtained from equations (7)–(10) using parameters in Table 1. Yellow and blue lighter shades represent 95% confidence intervals.

Table 1
Parameters in Equations (7)–(10)

Parameter	Equation	X_1 [a]	X_2 [a]	X_3 [a]	X_4 [a]	*R*-square
Please find the equation (5) for the correct one.The "m" is superscript, the "n, p" is subscript, the "m" is above the "n, p".Cm n,p	7	−0.911	0.414	21.85	0.672	0.997
Please find the equation (6) for the correct one.The "m" is superscript, the "p" is subscript, the "m" is above the "p". Cm p	8	−0.121	1.121	18.78	0.942	0.955
$D_{n,p}$	9	−0.136	1.251	18.19	1.000[b]	0.978
D_p.	10	0.060	0.891	22.78	0.082	0.907

Note. R-square represents the goodness of fitting.
[a]X_i where i = 1–4 represent G_i, H_i, J_i and K_i for *Please find the equation (5) for the correct one.The "m" is superscript, the "n, p" is subscript, the "m" is above the "n, p".Cm n,p, Please find the equation (6) for the correct one.The "m" is superscript, the "p" is subscript, the "m" is above the "p".Cm p*, $D_{n,p}$ and D_p, respectively. [b]Upper boundary J_4 in Equation (9) was fixed as 1.000 in this study to ensure $D_{n,p}$ no more than 1.

subscript, the "m" is above the "p".Cm p, $D_{n,p}$ and D_p is similar to G_i for *Please find the equation (5) for the correct one.The "m" is superscript, the "n, p" is subscript, the "m" is above the "n, p".Cm n,p.*

2.3.2. Model Reparametrization

As discussed in sections 2.1 and 2.2.1, 23 samples (matchups) were removed from 262 samples for independent model validation, leaving 239 samples for model parametrization. Size-fractionated concentrations and percentages are plotted as a function of total chlorophyll-a concentration, with the color representing SST in Figure 2. The model is seen to capture the general trends in the size-fractionated percentages and concentrations, except that it overestimated some samples at high total chlorophyll-a concentrations and low temperatures, with in situ nanoplankton and picoplankton concentrations lower than 0.1 and 0.01 mg/m^3, respectively (Figures 2c and 2d). Furthermore, SST has a clear influence on distribution patterns of PSCs, with lower SST leading to higher percentages of microplankton, lower percentages of nanoplankton and picoplankton under similar total concentrations. Further confirmation was found when the unknown model parameters (i.e., *Please find the equation (5) for the correct one.The "m" is superscript, the "n, p" is subscript, the "m" is above the "n, p".Cm n,p*, *Please find the equation (6) for the correct one.The "m" is superscript, the "p" is subscript, the "m" is above the "p".Cm p*, $D_{n,p}$, and D_p) obtained by fitting equations (5) and (6) using nonlinear least-square regressions (MATLAB R2014b) separately to lower SST waters (<22.45 °C, N = 140) and higher SST waters (>22.45 °C, N = 99). Estimates by SST-independent three-component model with fixed parameters for low and high SST are shown in Figure 2, indicating model parameters vary with SST.

We sorted the data set and conducted a 140-point running fit of equations (5) and (6) using nonlinear least-square regressions (MATLAB R2014b) as a function of SST. During fitting, we set parameter $D_{n,p}$ to 1 if $D_{n,p} > 1$ when SST were lower (Figure 3b). One hundred sets of SST and corresponding *Please find the equation (5) for the correct one.The "m" is superscript, the "n, p" is subscript, the "m" is above the "n, p".Cm n,p*, *Please find the equation (6) for the correct one.The "m" is superscript, the "p" is subscript, the "m" is above the "p".Cm p*, $D_{n,p}$, and D_p were obtained, and their relationships could be represented by equations (7)–(10); thus, parameters were fitted using nonlinear least-square regressions (MATLAB R2014b), as shown in Table 1.

Based on the in situ parameterization data set in this study and method in Sun et al. (2018), an SST-independent three-component model with fixed parameters (Brewin et al., 2010, 2015) was reparametrized, of which *Please find the equation (5) for the correct one. The "m" is superscript, the "n, p" is subscript, the "m" is above the "n, p".Cm n,p*, *Please find the equation (6) for the correct one.The "m" is superscript, the "p" is subscript, the "m" is above the "p".Cm p*, $D_{n,p}$, and D_p were 0.478 mg/m^3, 0.086 mg/m^3, 0.998, and 0.129, respectively. In comparison, the performance for all size classes improved when using SST-dependent three-component model (Figure 4). Modeled *Please find the equation (5) for the correct one.The "m" is superscript, the "n, p" is subscript, the "m" is above the "n, p".Cm n,p* and *Please find the equation (6) for the correct one.The "m" is superscript, the "p" is subscript, the "m" is above the "p".Cm p* in the SST-

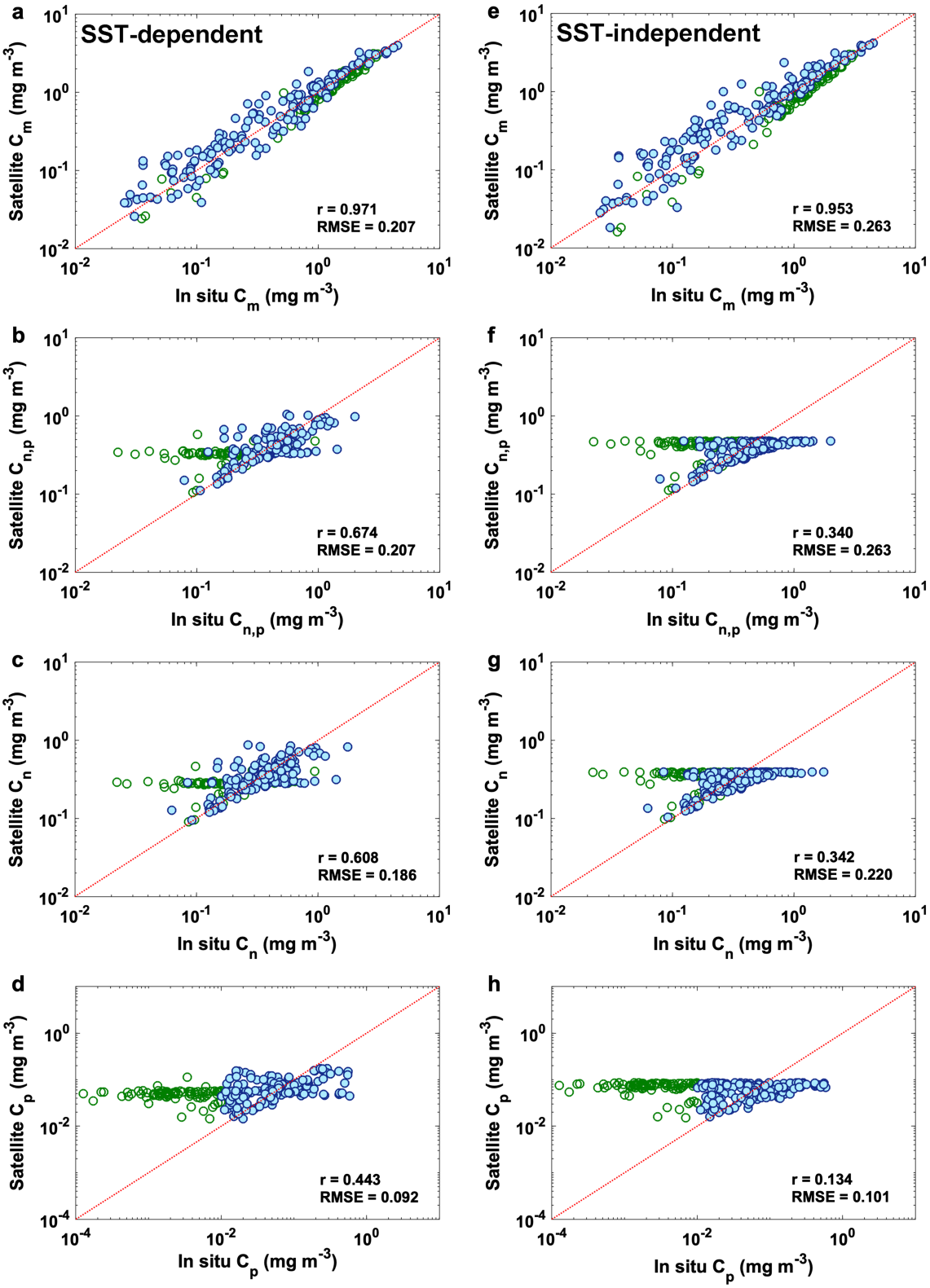

Figure 4. Comparison between in situ measurements (x axis) and estimated size-fractionated concentrations (y axis) in parametrization data set ($N = 239$), derived from SST-dependent three-component model (left column) and SST-independent three-component model (right column), respectively. Samples of which in situ picoplankton concentrations higher than 0.01 mg/m^3 were shown in filled blue symbols, while ones lower than 0.01 mg/m^3 were shown in hollow green symbols.

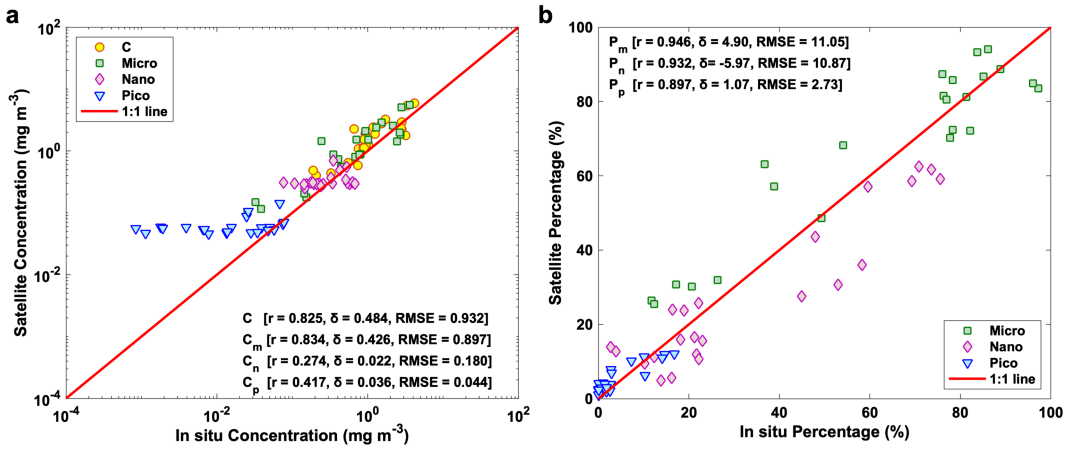

Figure 5. Validation of total and size-fractionated chlorophyll-a concentrations (a) and size-fractionated percentages (b). Solid lines represent the 1:1 lines. The units of δ and RMSE are mg/m^3 in (a), and % in (b).

independent model tended to reach unrealistic static asymptotes at high chlorophyll-a concentrations (Figures 4e–4h), whereas, the SST-dependent model captured better variability at higher chlorophyll-a concentrations and had better performance (i.e., lower root mean square error (RMSE)), especially for nanoplankton, picoplankton and the sum of nanoplankton and picoplankton (Figures 4a–4d). Even so, there were still data that the SST-dependent model did not capture well, related to extremely low chlorophyll-a concentrations of picoplankton in this work (<0.01 mg/m^3, hollow circles in Figure 4). Both versions of three-component models struggled to capture variations in picoplankton as a function of chlorophyll-a concentration, as explained by dispersed values of in situ picoplankton concentration in this comparison (Figure 2d).

2.4. Statistical Tests

Parameters including the bias (δ) and RMSE are used to compare in situ measurements and satellite estimations. The δ and RMSE were calculated according to

$$\delta = \frac{1}{N}\sum_{i=1}^{N}\left(X_{i,A}-X_{i,B}\right), \tag{11}$$

and

$$RMSE = \left[\frac{1}{N}\sum_{i=1}^{N}\left(X_{i,A}-X_{i,B}\right)^2\right]^{1/2}, \tag{12}$$

where, N is the number of samples and X is variable (e.g., chlorophyll-a concentration, percentages of PSCs) derived from satellite estimations (subscript A) and in situ measurements (subscript B). Pearson linear correlation coefficient (r) and p value (p) are used for judging the correlations between: (1) estimations and measurements; and (2) PSCs and environmental factors.

3. Results

3.1. Satellite Validation

Independent matchups (N = 23) were used for validating the performance of SST-dependent three-component model (equations (5)–(10)). These in situ measurements were matched with daily OC-CCI chlorophyll-a concentration and OISST products using a 3-by-3 pixel window closest to the location. The OC-CCI chlorophyll-a and OISST data were used as input to the model, and resultant SST-dependent modeled PSCs were compared with in situ PSCs. Figure 5a showed that satellite-derived total and microplankton chlorophyll-a concentration were in good agreement with in situ data, with r = 0.825 and 0.834, respectively. Bias indicated that the reparametrized three-component model overestimated total and size-fractioned

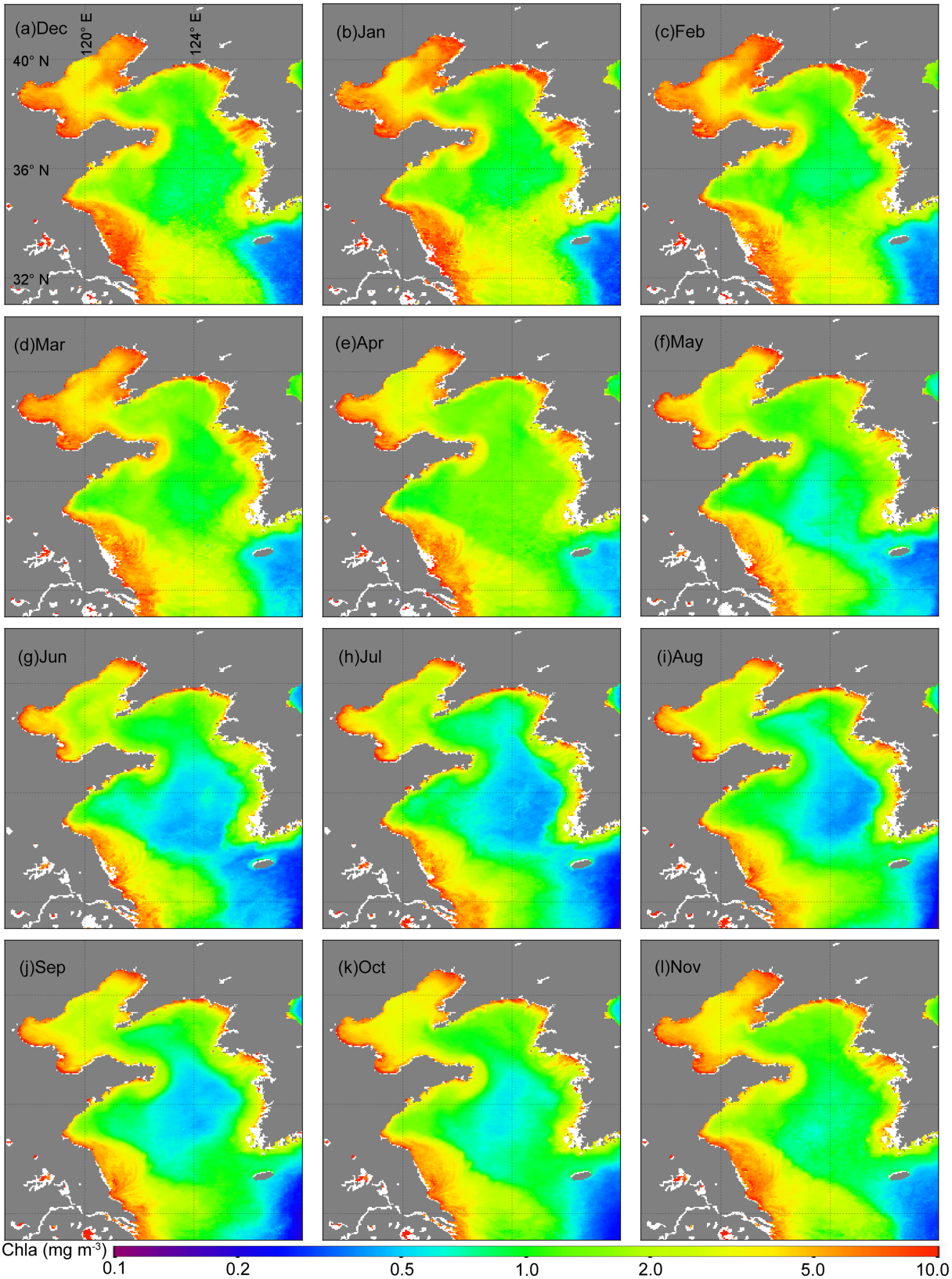

Figure 6. Monthly-averaged OC-CCI chlorophyll-a concentration images from September 1997 to December 2016 in the BS and YS.

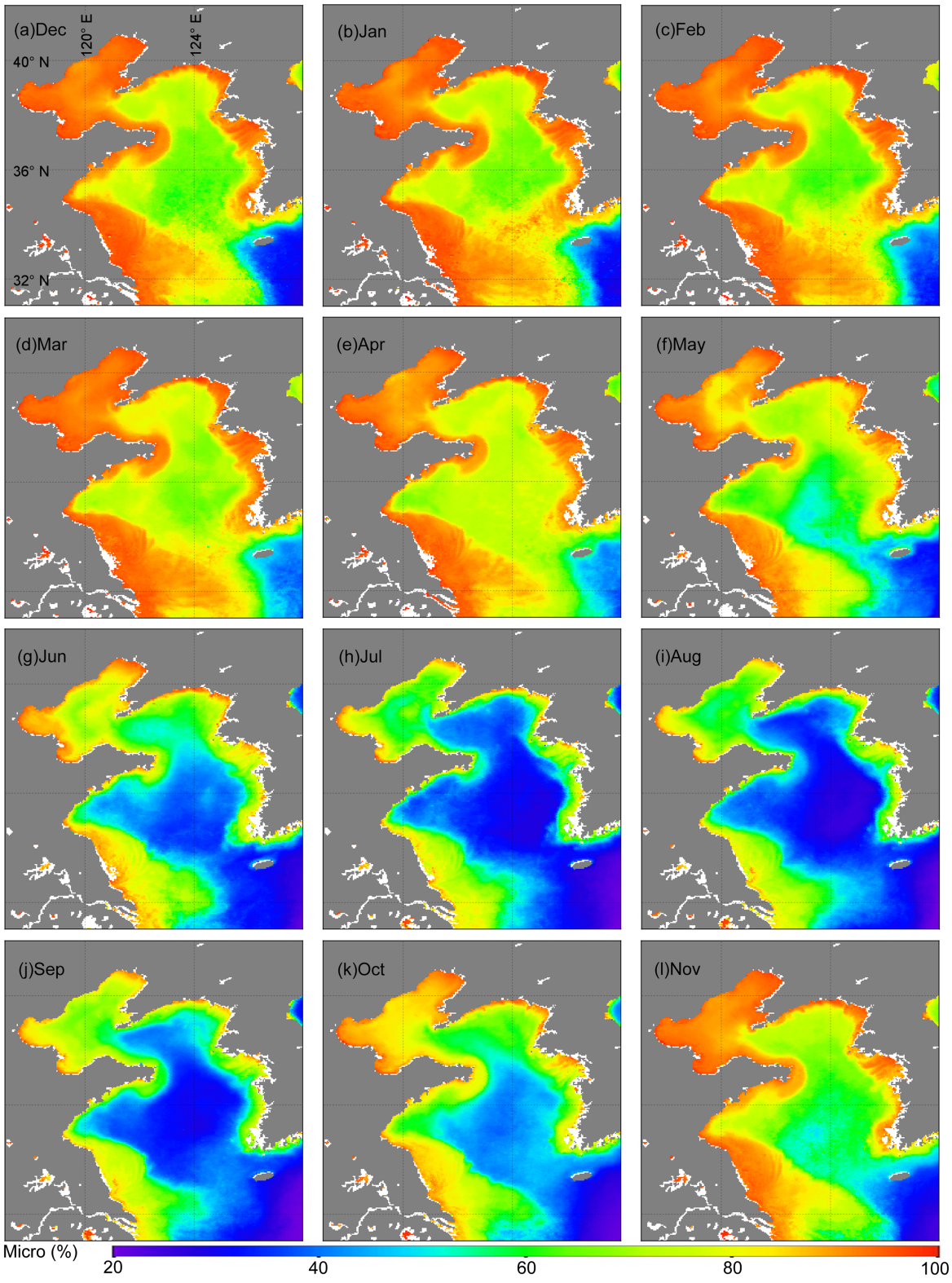

Figure 7. Monthly-averaged microplankton percentages derived from OC-CCI chlorophyll-a data from September 1997 to December 2016 using the SST-dependent three-component model.

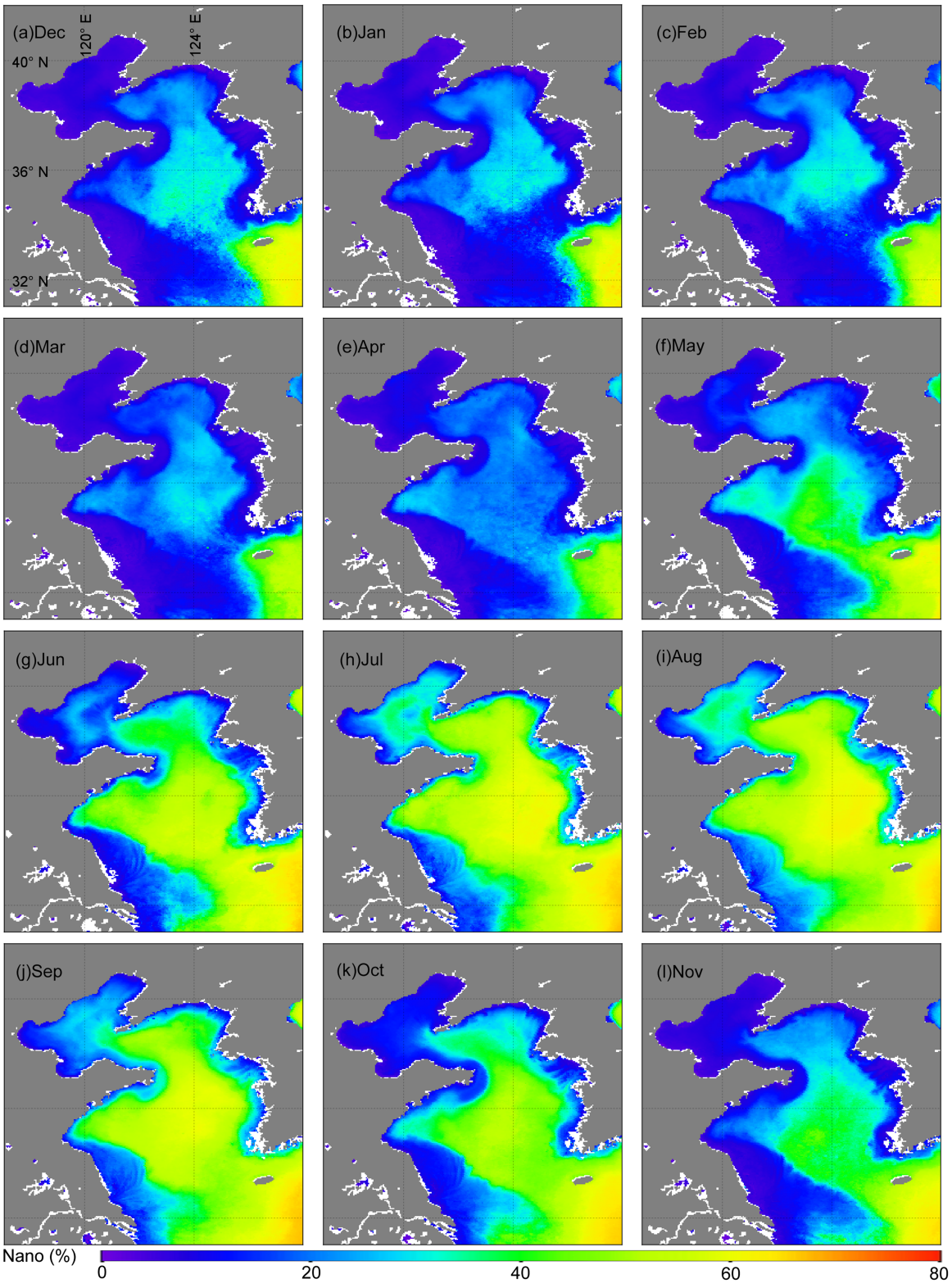

Figure 8. Monthly-averaged nanoplankton percentages derived from OC-CCI chlorophyll-a data from September 1997 to December 2016 using the SST-dependent three-component model.

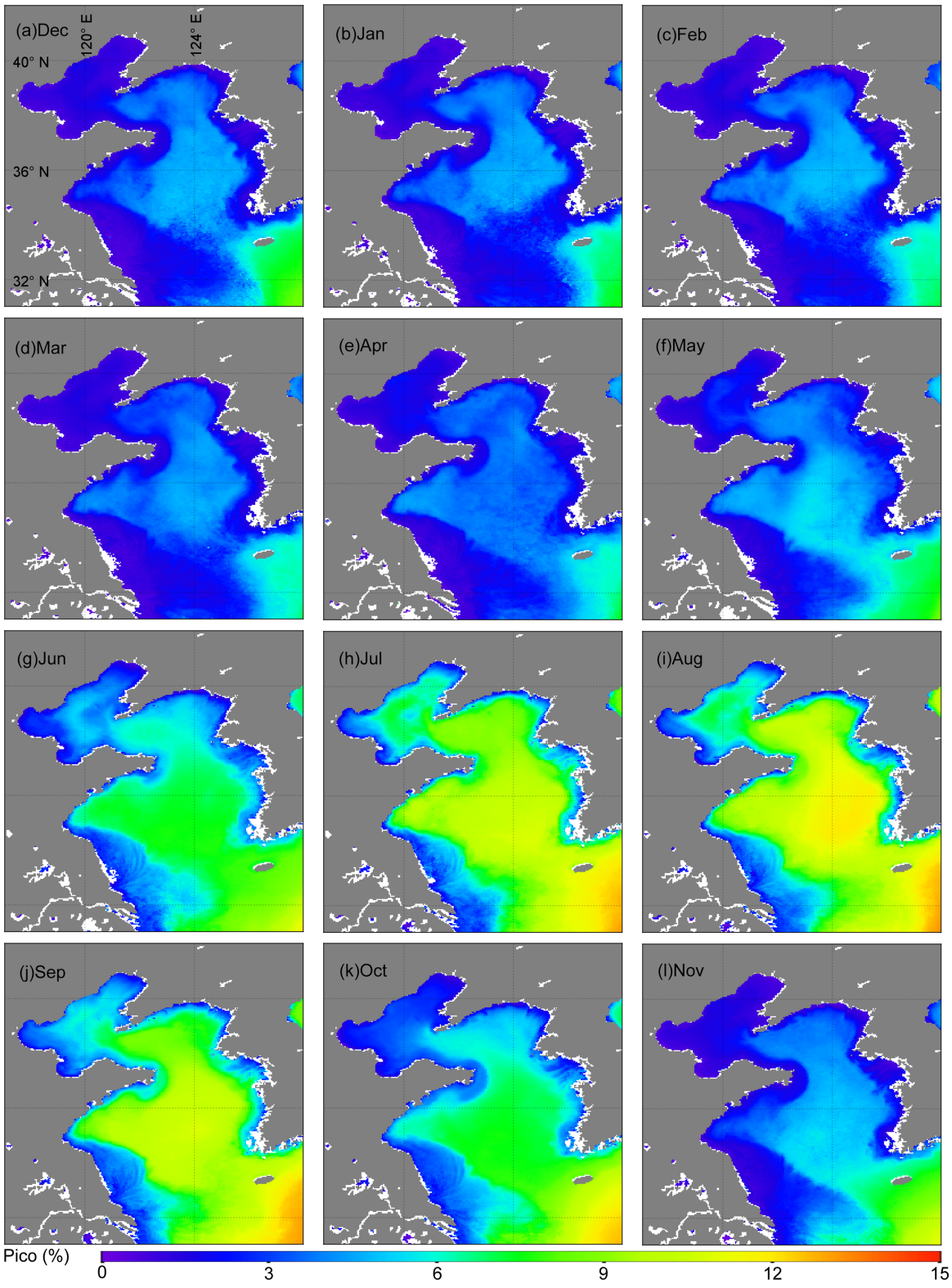

Figure 9. Monthly-averaged picoplankton percentages derived from OC-CCI chlorophyll-a data from September 1997 to December 2016 using the SST-dependent three-component model.

microplankton and nanoplankton concentrations slightly. Due to the extremely low in situ picoplankton measurements, variations between total chlorophyll-a concentration and picoplankton concentration were hard to capture (Figure 4d), which could explain the high positive bias between in situ and SST-dependent model derived picoplankton concentrations. As for size-fractionated percentages, satellite estimations compared well with the in situ data (Figure 5b), with considerably higher correlations.

3.2. Monthly Variation of Chlorophyll-a Concentration and PSCs

3.2.1. Bohai Sea and Yellow Sea

Monthly chlorophyll-a concentration (Figure 6) exhibited regional differences in the entire study area, both in very productive water with high chlorophyll-a concentrations and in oligotrophic water with low chlorophyll-a concentrations. Throughout the year, chlorophyll-a concentration values >2 mg/m^3 were observed in nearshore area of the BS and YS, while lower values (<2 mg/m^3) were found over most of the offshore area in the north YS (NYS) and SYS. Microplankton comprised over 40% of total chlorophyll-a concentration in the coastal regions, with 20–60% in the central YS (Figure 7). In contrast, nanoplankton proportion did not exceed 50% in shelf regions, while in the offshore area, the highest percentages were up to 70% (Figure 8). Picoplankton rarely contributed along coasts, but had relatively higher percentages in the offshore domain (Figure 9).

In the entire BS, coastal regions of the NYS (i.e., northern Shandong peninsula) and SYS (i.e., northern Jiangsu province), similar monthly variations with different value ranges of chlorophyll-a concentration and PSCs percentages were found (Figures 6–9). Higher chlorophyll-a concentration values were observed from December to March, and since then, an obvious decrease led to the lowest value in July. Microplankton comprised over half of the total chlorophyll-a concentration, with the minimum proportion in July and August. Nanoplankton and picoplankton proportions were 5–50% and no more than 10%, respectively, with much higher proportions observed from July to September.

In contrast to shelf regions, the Changjiang estuary region (~31°N, 122.5°E) showed lower chlorophyll-a concentration in January, February, and March (Figure 6). Highest concentrations were seen in July, likely due to the rapid growth of phytoplankton from June to August. Although microplankton was dominant throughout the year (>60%), slight monthly variation in the percentages of nanoplankton (5–30%) and picoplankton (0–10%) were observed, with maximum proportions from August to October (Figures 7–9).

The central NYS and central SYS exhibited similar monthly variations, where chlorophyll-a concentration increased from December, with a peak in April (Figure 6). Since then, values declined with the lowest value observed in July and August. Similar to other areas, microplankton were dominant for the most of year, except from June to October (Figure 7). During this period, nanoplankton percentages exceeded microplankton and became dominant, comprising 40–70% of total chlorophyll-a concentration (Figure 8). Picoplankton percentages remained below 15% throughout the year. However, relative high proportions were sustained from June to October, compared with low values in other regions (Figure 9).

3.2.2. 36°N Transect

Figure 10. shows monthly-averaged chlorophyll-a concentration and size-fractionated PSCs along the 36°N transect (Figure 1b), presenting variations in surface water where bottom YSCWM may impact in the SYS.

West of 122°E, a low chlorophyll-a concentration area (<1 mg/m^3) started to form along the transect in April, and its boundary could extend as far west as 121°E in July (Figure 10a). After that, chlorophyll-a concentration increased and was seen to be higher than 1 mg/m^3 from October. In comparison, in the eastern part of the transect, chlorophyll-a concentration was much higher in April but dropped significantly by May, falling from around 1.5 to less than 1 mg/m^3. The low values of chlorophyll-a concentration lasted until November and covered an area as far east as 126°E. In general, chlorophyll-a concentrations were much lower in the eastern area than the western part. The lowest values were centered along the 36°N transect located nearby 121.3°E (~0.7 mg/m^3) in June and July and nearby 125°E (~0.4 mg/m^3) in July and August, respectively.

Similarly, microplankton contribution in the eastern part of the transect was lower than the western part throughout the year (Figure 10b). To the west of 122°E, microplankton comprised over 70% of the chlorophyll-a concentration from November to April with percentages decreasing to 30–60% between May and October. In the eastern area, microplankton contribution was around 50–70% from November and

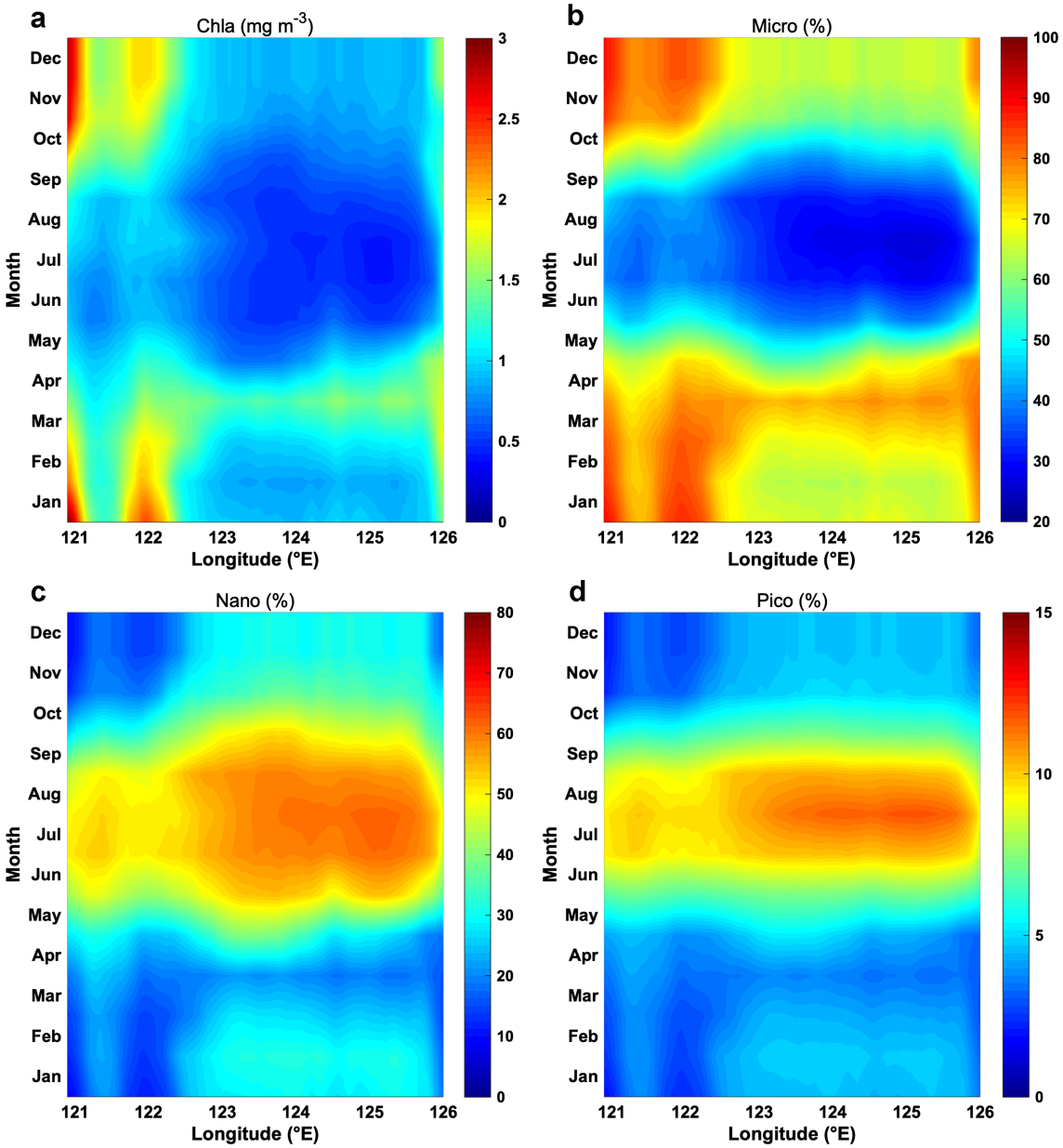

Figure 10. Monthly-averaged variations of chlorophyll-a concentration (a) and size-fractionated percentages (b–d) in the 36°N transect from September 1997 to December 2016.

March and much higher in April (over 70%). By May, the contribution decreased, and lower values occupied most of the 36°N transect, reaching as low as 25% in the eastern area in August.

Compared with microplankton, an inverse distribution of monthly variations was observed for nanoplankton, with much higher fractions in the eastern 36°N transect than the western area (Figure 10c). From November to April, nanoplankton contributed 10–40% of the chlorophyll-a concentration, whereas they dominated the chlorophyll-a concentration between May and October over most of the transect, with one western peak (>50%) in July and one eastern peak (>60%) in August.

Picoplankton percentages were much lower from November to May, which were no more than 5% over most of 36°N transect (Figure 10d). Higher proportions of picoplankton were found from June to October, ranging from 5% to 15%. High values of picoplankton contributions were mainly concentrated in the eastern area of the transect.

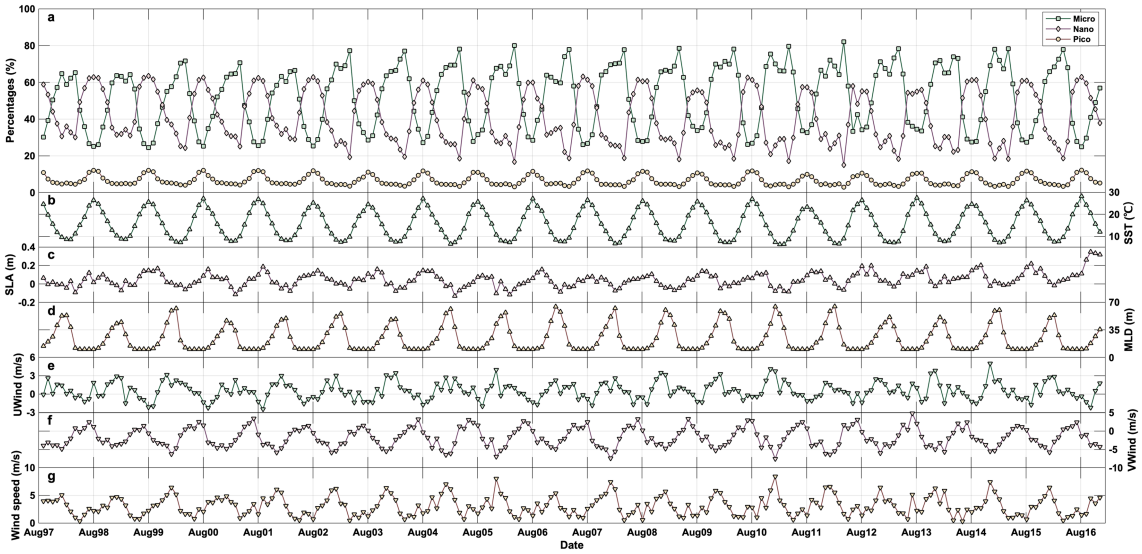

Figure 11. Monthly variations of size-fractionated percentages (a) and environmental factors, which include SST (b), SLA (c), MLD (d), UWind (e), VWind (f) and wind speed (g) from September 1997 to December 2016 in the selected ROI region in the SYS.

These observations of PSCs variations in the surface water were likely due to a transition from a well-mixed water column in winter to a stratified one in summer caused by YSCWM in the central SYS. More detailed analyses about physical and ecological interactions can be found in sections 3.2.3 and 4.2.2.

3.2.3. Physical Interactions and Correlation Analysis

To investigate how environment factors influence PSCs, monthly time series (i.e., from September 1997 to December 2016) of surface size-fractionated percentages, SST, SLA, MLD, and CCMP vector winds in central SYS (ROI in Figure 1b) were compared, as shown in Figure 11 and Table 2. Mean value were calculated for the selected surface area where the bottom YSCWM exists.

Monthly averaged SST (Figure 11b) has a maximum in August (~26 °C) and minimum in February (~7 °C). Similar seasonal cycles are found in the monthly variations of SLA (Figure 11c), with high positive SLA occurring in August (~0.1 m) and high negative SLA in March (~−0.03 m). Higher MLD were found in January and February (~55 m), while from May to August, MLD tended to be about 10 m over last 20-year period (Figure 11d). Seasonal wind cycles in selected area were shown in Figures 11e–11g. The zonal component (i.e., UWind) indicated that from August and September, winds originating from east started to change the direction, leading to the strongest westerly winds in December and January. The meridional component (i.e., VWind) showed a much clearer pattern with direction changing. In July (December), southerly (northerly) winds were the strongest, after which wind speeds gradually weakened. The wind speeds (scaler quantity) were calculated from two vector winds data, with highest speed observing in January (~5 m/s^1) and lowest in April (~1 m/s^1).

Table 2
Correlation Analysis Between Environmental Factors and SST-dependent Model Derived Size-Fractionated Percentages

Environmental factors	Pearson linear correlation coefficient (r)		
	Microplankton	Nanoplankton	Picoplankton
SST (N = 232) (SST-dependent)	−0.937	0.929	0.930
SST (N = 232) (SST-independent)	−0.790	0.791	0.781
SLA (N = 232)	−0.607	0.608	0.570
MLD (N = 232)	0.611	−0.611	−0.578
UWind (N = 232)	0.628	−0.622	−0.621
VWind (N = 232)	−0.430	0.426	0.429
VWind (N = 231) (1 month interval)	−0.743	0.734	0.749
Wind speed (N = 232)	0.291	−0.290	−0.284
Wind speed (N = 231) (1-month interval)	0.548	−0.555	−0.480

Note. Correlation analysis between environmental factors and SST-independent model derived size-fractionated percentages, 1-month interval for VWind, and wind speed were included for comparison. p Values are smaller than 0.01 for all correlation analysis listed above.

It can be seen from both Figure 11 and Table 2 that variations in environmental factors and PSCs are tightly connected. Monthly microplankton percentages were negatively correlated with SST and SLA, whereas nanoplankton and picoplankton percentages were positively correlated with these variables. Opposite correlations were found between MLD and PSCs, indicating that higher stratification (i.e., lower MLD) would lead to low proportions of microplankton and high proportions of both nanoplankton and picoplankton. Pearson linear correlation coefficient (r) in Table 2 indicated that

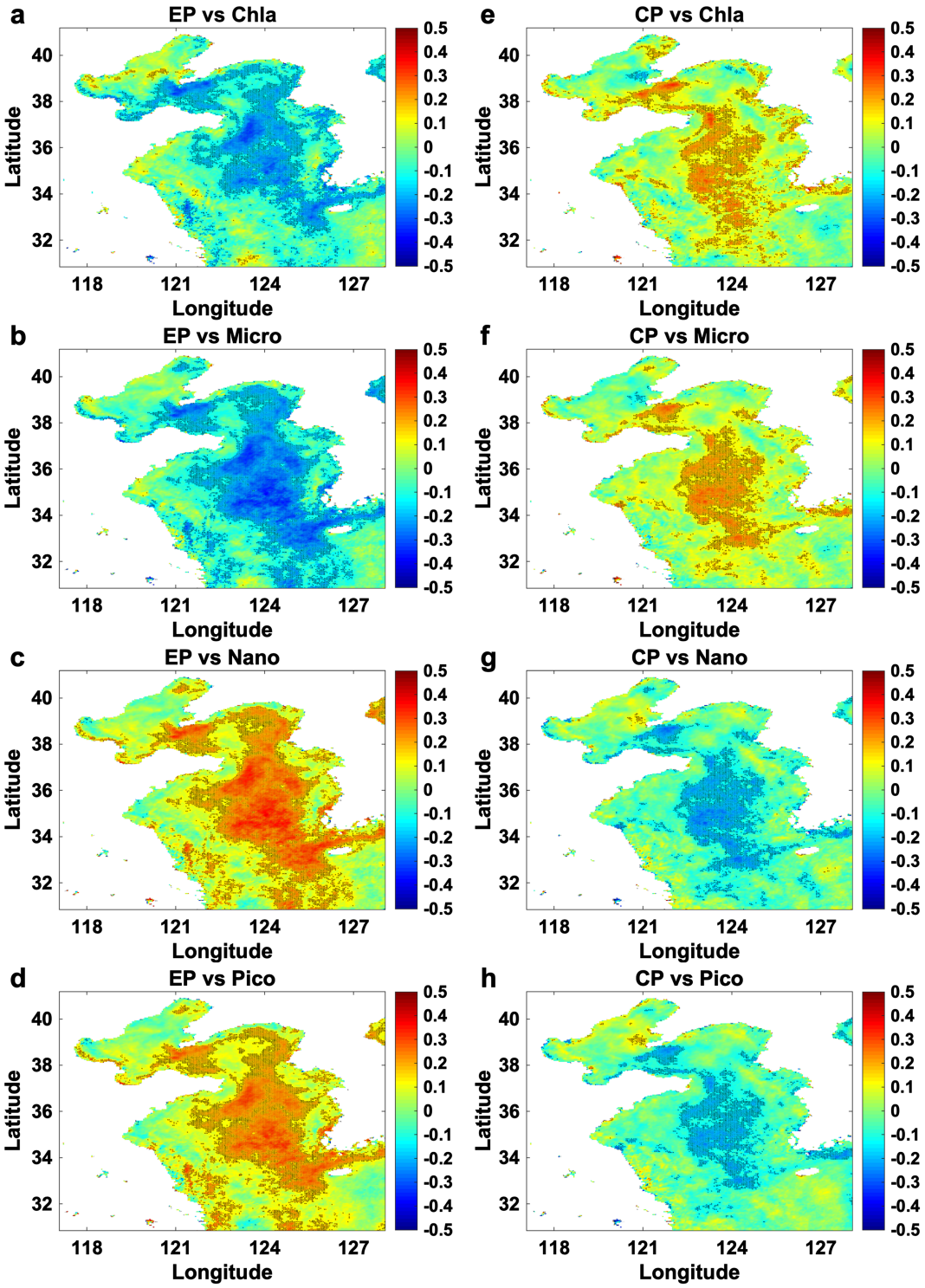

Figure 12. Correlation maps between Eastern Pacific (EP), Central Pacific (CP) El Niño indices, and surface monthly anomalies in chlorophyll-a concentration and percentages of PSCs over the period from September 1997 to December 2016, on a pixel-by-pixel basis. Black dots indicate where correlations were significant with p value < 0.05, $N = 232$.

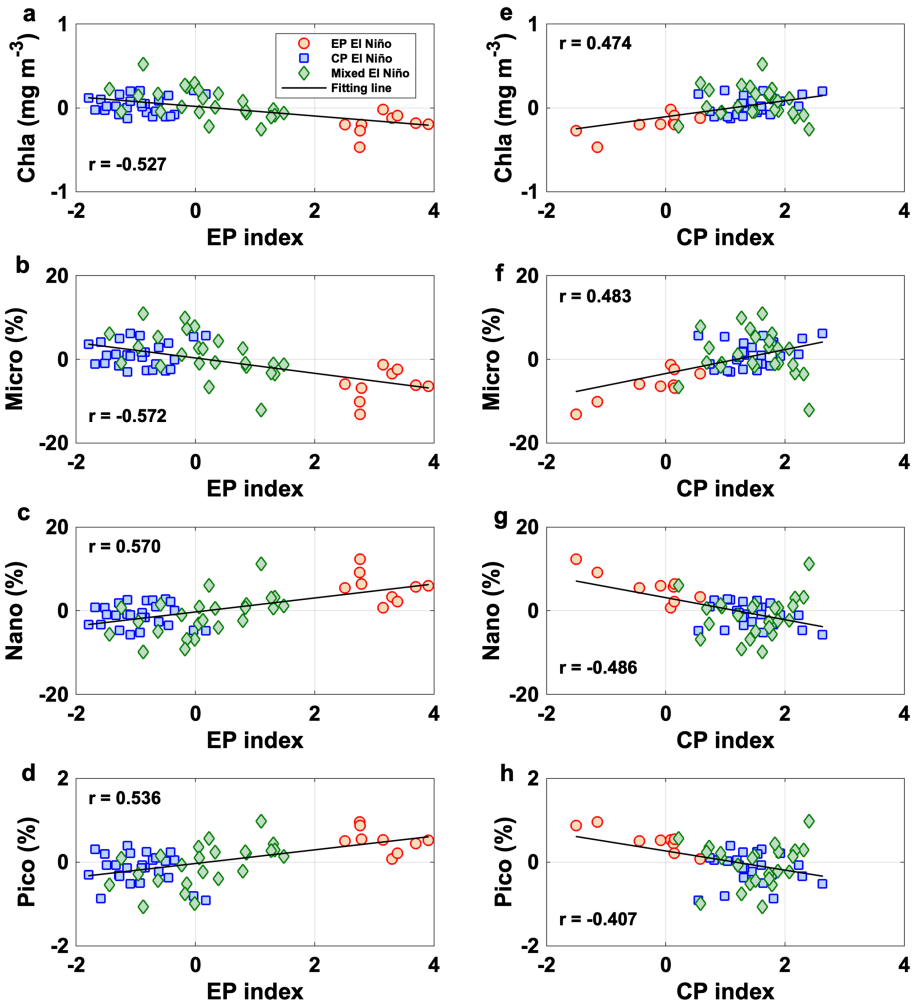

Figure 13. Relationships between Eastern Pacific (EP), Central Pacific (CP) El Niño indices and surface monthly anomalies in chlorophyll-a concentration and percentages of PSCs during different El Niño events (ONI index ≥0.5). Trend lines are shown in black and p values are smaller than 0.01 for all correlation analysis shown in the figure, with $N = 59$.

both wind direction and wind speed influenced variations in PSCs. When easterly and southerly winds prevailed, there were higher proportions of nanoplankton and picoplankton, which was the case in the August. By contrast, westerly and northerly winds were more likely to lead to high percentages of microplankton. Wind speeds were positively correlated with microplankton and negatively correlated with nanoplankton and picoplankton. Clear 1-month hysteresis effects were found in size-fractionated percentages, when comparing with the VWind and wind speed (Table 2).

Naturally, correlations between SST and size-fractionated percentages are impacted by the SST-dependent parametrization of three-component model. Therefore, PSCs percentages derived from SST-independent three-component model with fixed parameters (details in sections 2.3.2 and 4.1) were calculated for comparison at the same time (Table 2), and did show a slight decline in correlations, but were still highly correlated.

3.3. Interannual Variation of Chlorophyll-a Concentration and PSCs

Monthly anomalies of chlorophyll-a concentration, PSCs, SST, SLA, MLD, and CCMP winds data were calculated by subtracting each monthly composite from corresponding climatological monthly means over the period 1997–2016, with the aim to compare their interannual relationships. In order to understand the response of climate variability on the size structure, monthly EP and CP indices were regressed against monthly anomalies in these biological and physical variables in the entire BS and YS, on a pixel-by-pixel

Table 3
Comparison of Size-Fractionated Concentrations and Percentages Between SST-Dependent and SST-Independent Three-Component Models Using Independent matchups, N = 23

	SST-dependent			SST-independent		
Parameters	r	δ	RMSE	r	δ	RMSE
Micro (%)	0.946	4.90	11.05	0.843	5.14	17.11
Nano (%)	0.932	−5.97	10.87	0.832	−6.32	15.27
Pico (%)	0.897	1.07	2.73	0.752	1.18	3.93
Micro (mg/m^3)	0.834	0.426	0.897	0.811	0.395	0.891
Nano (mg/m^3)	0.274	0.022	0.180	0.198	0.043	0.180
Pico (mg/m^3)	0.417	0.036	0.044	−0.385	0.046	0.057

basis. As shown in Figure 12, significant correlations between EP/CP indices versus monthly anomalies of chlorophyll-a concentration and percentages of PSCs were mainly observed in the central SYS and Bohai strait area ($p < 0.05$, $N = 232$). Compared with the CP index, the EP index explained a higher amount of variability in the size structure with a higher significance level. Monthly anomalies in chlorophyll-a concentration and microplankton percentage were negatively (positively) correlated with EP index (CP index), whereas positive (negative) correlations were observed between nanoplankton and picoplankton and EP index (CP index). We also analyzed and plotted correlation maps for all the physical variables but did not find significant correlations with EP/CP indices, except for the relationship between SST and the EP index, which is mentioned below.

To investigate further which physical variables influenced the size structure, correlations between monthly anomalies in chlorophyll-a concentration and PSCs versus anomalies in all the physical variables were calculated in the central SYS (ROI in Figure 1b). During the entire period ($N = 232$), anomalies in SST were correlated with anomalies in chlorophyll-a concentration ($r = -0.258$, $p < 0.01$) and the SST-dependent model derived microplankton ($r = -0.400$, $p < 0.01$), nanoplankton ($r = 0.369$, $p < 0.01$), and picoplankton ($r = 0.588$, $p < 0.01$). In comparison, by removing the impacts of SST in the SST-dependent model, anomalies in SST had slightly lower but still significant correlations with anomalies in the SST-independent model derived microplankton ($r = -0.240$, $p < 0.01$), nanoplankton ($r = 0.239$, $p < 0.01$), and picoplankton ($r = 0.246$, $p < 0.01$). No significant correlations were found between monthly anomalies in other physical variables and anomalies in size structure. Moreover, anomalies in SST were positively correlated with the EP index ($r = 0.206$, $p < 0.01$, $N = 232$), and no significant correlations were found with the CP index, indicating that interannual variations of SST caused by climate variability could explain some of the variation in the size structure.

Results from Figure 13 showed tight correlations between different El Niño events (i.e., monthly ONI index ≥ 0.5, $N = 59$) and variations in chlorophyll-a concentration and percentages of PSCs. During the EP El Niño event, EP index (CP index) were larger (smaller), leading to negative (positive) anomalies in chlorophyll-a concentration and percentages of microplankton (nanoplankton and picoplankton). When CP and mixed El Niño events happened, both positive and negative anomalies in chlorophyll-a concentration and size structure were observed. However, values of anomalies were higher than EP El Niño events and tended to be positive (negative) for chlorophyll-a concentration and percentages of microplankton (nanoplankton and picoplankton).

4. Discussion

4.1. Satellite Inputs and SST-Dependent Three-Component Model

The stability and accuracy of satellite-derived chlorophyll-a concentration (OC-CCI, version 3.1) and SST (OISST, version 2) as inputs are required for analyzing variations of PSCs in the 20-year satellite time series. Due to the finite life span of satellite sensors, long timescale studies on chlorophyll-a concentration relied on successive missions of ocean color data, such as the SeaWiFS and MODIS (He et al., 2013; Liu & Wang, 2013; Sun et al., 2019). Through analysis, we observed differences in intermission (i.e., SeaWiFS and MODIS) chlorophyll-a concentration (not shown), which could lead to spurious conclusions in long timescale researches (Mélin, 2016). In contrast, the multimission OC-CCI chlorophyll-a concentration has proven to be consistent with single-mission data set (Mélin et al., 2017), creating an advantage for multiannual analysis in climate-change studies (Sathyendranath et al., 2017). Moreover, the OC-CCI chlorophyll-a concentration has been validated extensively with large amount of independent in situ measurements from open ocean to regional areas (Brewin et al., 2017, 2016, 2015; Gittings et al., 2017; Racault et al., 2015). A significant relationship ($r = 0.825$, $p < 0.001$) between OC-CCI chlorophyll-a concentrations and independent in situ measurements was observed in the study (Figure 5a), though a slight overestimation in satellite-derived values was evident, probably due to difficulties in remotely sensing chlorophyll-a data in optically complex

waters (IOCCG, 2000). However, statistics in the results showed that the OC-CCI chlorophyll-a concentration in the BS and YS was comparable with the performances of other chlorophyll-a algorithms in the same study area (Cui et al., 2010; He et al., 2013; Sun et al., 2019, 2018), providing confidences in the use of OC-CCI chlorophyll-a concentration data in the study. As for SST, the result of validation in the study showed high accuracy ($r = 0.971$, $p < 0.001$, $N = 23$), and in recent years, OISST data sets have been applied extensively in various oceanic regions (Brewin et al., 2017; Friedland et al., 2018; González Taboada & Anadón, 2014; Liu & Wang, 2013), suggesting a maturity for long timescale research.

Statistics tests of validation between in situ data and satellite estimations using SST-dependent and SST-independent models were shown in Table 3. When using SST-dependent three-component model, the performance improved for all size-fractionated concentrations and percentages (Table 3), especially for nanoplankton and picoplankton, compared with that using a fixed set of parameters. Differences between the two versions of the three-component models (i.e., SST-dependent and SST-independent) were consistent with previous work (Brewin et al., 2017), indicating an improvement in model performance was achieved by introducing parameter variations with SST. Moreover, based on global in situ PSCs data set, using a different technique to HPLC, size-fractionated successive filtration matched with concurrent SST, Ward (2015) found that cold waters supported a larger proportion of microplankton and led to a reduction of picoplankton at similar chlorophyll-a concentrations. Relationships between total chlorophyll-a concentration, size structure, and SST (see their Figure 2) were similar to those in this study (Figure 2), suggesting an SST-dependent model will lead to a better performance when estimating PSCs.

However, the SST-dependent model still overestimated picoplankton concentrations (Figure 5a), which was likely due to (1) the slightly positive bias for satellite-derived total chlorophyll-a concentration (Figure 5a), which were the input to the model; and (2) the model was not able to capture the variations of picoplankton concentration at high total chlorophyll-a concentration (e.g., 1 mg/m^3) and low temperature (e.g., 15 °C, Figure 2d), resulting in unrealistic asymptotes when in situ picoplankton concentrations were lower than 0.01 mg/m^3 (Figure 4d). Therefore, the SST-dependent model could overestimate picoplankton concentrations in the nearshore areas, especially in cold seasons. However, in the central SYS (e.g., ROI in Figure 1 b), total chlorophyll-a concentration were lower than 1 mg/m^3 throughout the year (Figure 6), and at the same time, satellite estimates and in situ percentages of PSCs were well correlated and had low biases (Figure 5b). Therefore, the SST-dependent model is likely to have little impact on the monthly and interannual variations of percentages of PSCs and their relationships with physical factors, as analyzed in sections 3.2.3 and 3.3.

In this study, we excluded the 22 samples with chlorophyll-a concentrations higher than 5 mg/m^3 during the reparametrization of the SST-dependent model. Compared to the rest of the samples, these 22 samples had higher temperatures, higher percentages and concentrations of microplankton, and lower percentages and higher concentrations of nanoplankton and picoplankton (not shown), meeting the assumption of the three-component model, which is that large cells always dominate at high chlorophyll-a concentrations and small cells at low concentrations. However, there is a possibility that the model could fail in estimating PSCs in blooms, if the relationships between size-fractionated and total chlorophyll-a concentrations are different from the trends observed in this study (Figure 2).

4.2. Spatial and Temporal Variations of Chlorophyll-a Concentration and PSCs

4.2.1. Bohai Sea and Coastal Yellow Sea

The spatial and temporal distribution of satellite-derived chlorophyll-a concentration and PSCs in this study are in agreement with previous in situ observations and remote sensing estimations (Fu et al., 2010, 2009; Huang et al., 2010; Sun et al., 2017, 2019, 2002, 2012, 2018). High chlorophyll-a concentration and large cell phytoplankton biomass were observed in entire BS and nearshore YS (Figures 6 and 7). Meanwhile, the central YS exhibited relatively low chlorophyll-a concentrations and a smaller-sized phytoplankton community (Figures 8 and 9). These variations matched the spatial distribution of nutrients. It was found that river inputs, agriculture, and industrial behaviors along the coast caused high concentrations of nutrients (Wang et al., 2003; Yu et al., 2000), resulting in high biomass and favoring the dominance of microplankton in coastal waters (Fu et al., 2009). Our results were consistent with previous studies that smaller-sized phytoplankton typically dominated in oligotrophic waters, while larger-sized phytoplankton in eutrophic waters (Agawin et al., 2000; Gomes et al., 2018).

Monthly climatology (Figure 6) showed that higher chlorophyll-a concentration occurred from December to March in the entire BS and the coastal YS, while a maximum in April in the central YS and a July maximum in the Changjiang estuary area, which were in agreement with previous studies (Fu et al., 2009; Gao & Li, 2009; Liu & Wang, 2013; Sun et al., 2002; Yamaguchi et al., 2013). These distributions were mainly driven by the interactions of temperature, solar radiation, wind forcing, circulations, and nutients throughout the year (Jiang et al., 2019). In the BS and coastal YS, Shandong Peninsula coastal front and Yellow Sea coastal front were strongest from January to April (Huang et al., 2010). Combined with a strong northwesterly wind (Figures 11e and 11f), convectional mixing developed (deepening of the mixed layer), and nutrients were introduced to surface water from deep layers in coastal waters, supporting high phytoplankton biomass in the winter and early spring. Meanwhile, chlorophyll-a concentrations were lower in summer. which may result from the relatively weak fronts, higher stratification (shallowing of the mixed layer), the depletion of nutrients, and the existence of higher grazing pressure from zooplankton.

The Changjiang estuary showed a significant summer chlorophyll-a concentration peak from May to August (Figure 6), which coincided with the summer rainy season, controlled by the East Asian monsoon system. The Changjiang Diluted Water, with a large discharge of freshwater, strengthened and spread more northward and northeastward during summer, due to high precipitation and weaken winds (Chen, 2009; Hwang et al., 2014). Elevated terrestrial inputs were the main source of nutrients for phytoplankton, especially those of larger size, such as diatoms and dinoflagellates in the Changjiang estuary area and southern YS (Jiang et al., 2014; Xu et al., 2019; Zhou et al., 2008; Zhu et al., 2009). Similar effects of large eutrophic river discharge on phytoplankton biomass and community were also reported in other estuarine areas (e.g., Chakraborty & Lohrenz, 2015; Sin et al., 2000).

4.2.2. Central Yellow Sea

In previous studies, higher chlorophyll-a concentrations were observed in spring in the central SYS, with the dominance of microplankton consisting mainly of diatoms (Fu et al., 2009; Liu et al., 2015; Xuan et al., 2011). These findings are in agreement with what we observed along the 36° transect during March and April (Figure 10). The warm and saline Yellow Sea Warm Current, from the previous winter, intruded and met the cold and turbid coastal waters, resulting in high concentrations of nutrients in well-mixed waters (Jin et al., 2013; Lin et al., 2011; Liu et al., 2015), which was beneficial for growth of large-sized phytoplankton in spring. In addition, it has been reported that high biomass in the central YS was usually associated with an increase of solar radiance and a weak vertical density gradient, which provided a longer residence time for phytoplankton in the euphotic zone (Hyun & Kim, 2003).

In summer, prevalent southeasterly winds (Figures 11e and 11f) influenced horizontal advection of coastal and ocean currents, leading to a positive SLA in the central YS (Cai et al., 2015; Qiao, 2005). Previous studies showed that positive SLA was usually accompanied with a decrease in chlorophyll-a concentration and higher proportion of smaller-sized phytoplankton in the surface layer (Bricaud et al., 2012; Corredor-Acosta et al., 2018), which agreed with the observations in Figure 11c and confirmed the positive correlations between SLA and percentages of nanoplankton and picoplankton (Table 2). Moreover, due to the strong solar heating and weak wind forcing, shallow MLD took place in summer (Figure 11d), indicating the existence of a strong thermocline between the shallow mixed surface layer and deeper colder water (Fu et al., 2018). Stratification was found to be an important factor in controlling the surface phytoplankton biomass and community (Jiang et al., 2019), since the thermocline barrier prevented the transfer of nutrients from deeper water to the surface layer (Fu et al., 2018; Wang et al., 2014; Wei, Yu, et al., 2016; Xin et al., 2015), and at the same time, nutrients were depleted in the surface layer after the high biomass in spring, limiting the growth of larger-sized phytoplankton. Lower chlorophyll-a concentration and higher percentages of nanoplankton and picoplankton from May to October (Figure 10 and 11) were in accordance with previous observations (Fu et al., 2010, 2009).

From autumn onward, much cooler SST and a deeper thermocline (i.e., larger MLD) were observed in Figure 11b and 11d, indicating that the YSCWM was fading. Uniform water column structure with approximately a 50-m MLD occurred in winter, of which the increasing wind speed from summer (1–2 m/s^1) to winter (5–6 m/s^1) was an important factor (Shi & Wang, 2012). Compared with summer, higher nutrient concentrations in autumn and winter have been reported (Fu et al., 2010; Liu et al., 2015; Wei, Yu, et al., 2016), supporting the increase of larger-sized phytoplankton and total chlorophyll-a concentration in the

surface layer of central SYS (Figure 10 and 11), as well as the positive correlation between MLD/wind speed and microplankton (Table 2).

In summary, the temporal variations of satellite-derived monthly averaged PSCs and chlorophyll-a concentration were mainly driven by seasonal changes in the currents, surface winds, SST, mixed/stratified water conditions and nutrients. Conversely, monthly variation of PSCs can also reflect detailed YSCWM formation processes, with YSCWM emerging in May, maturing in August and gradually disappearing in October (Zhang et al., 2008). Moreover, remotely sensed estimations can provide more comprehensive information at a larger scale. Spatial distributions of phytoplankton biomass and size structure in the 36°N transect (Figure 10) coincided with the two cold cores of YSCWM located at the eastern and western part of SYS (Yu et al., 2006; Zhang et al., 2008; Zhu et al., 2018), which was not observed through previous in situ investigations.

4.3. Implications for Climate Impact

Previous studies found that El Niño events had impacts on global phytoplankton productivity and phytoplankton size structure (e.g., Behrenfeld et al., 2006; Kostadinov et al., 2010), and different physical-biological interactions were observed in EP and CP El Niño events (e.g., Gierach et al., 2012; Racault et al., 2017). Pixel-by-pixel correlations in Figure 12 provided robust evidence that impacts of El Niño on phytoplankton biomass and size structure could also reach the BS and YS, where chlorophyll-a concentration and PSCs were more sensitive to the EP index, supporting the findings that EP El Niño had a strong influence in the East Asia and western Pacific areas (Yuan & Yang, 2012). Based on a long time series satellite data, the influences of climate phenomenon on phytoplankton biomass and composition were found to be complicated, driven by a variety of environmental variables, including fluctuations in SST, sea surface height, stratification, and winds (Brewin et al., 2012; Gierach et al., 2012; Mouw et al., 2019; Racault et al., 2017).

In this study, monthly variations of size structure were highly correlated with physical variations (Figure 11 and Table 2); however, on interannual time scales, links between physical drivers and PSCs were much weaker. SST was found to be the major factor influencing the phytoplankton biomass and size structure in the central SYS. Positive correlation between anomalies in SST and the EP index in this study was consistent with anomalous SST warming in the YS during the 1997–1998 EP El Niño event (Tang et al., 2000; Wang et al., 2012). The effects of SST on variations of phytoplankton biomass and PSCs were probably associated with elevated (suppressed) nutrient vertical exchange, caused by surface cooling (warming) in higher latitude stratified waters (Behrenfeld et al., 2006; Boyce et al., 2010; Doney, 2006).

However, due to the superimposed impact of long-term global warming (IPCC, 2013) and spatial differences in interannual variations of chlorophyll-a and SST in the BS and YS (Liu & Wang, 2013), future responses to El Niño in the region are not clear. Furthermore, derived model parameters, which define the relationship between size-fractionated and total chlorophyll-a concentration in the region, computed from data collected in the past, could be vulnerable to changes in the future (Sathyendranath et al., 2017), potentially influencing the correlations between physical variables and size structure observed here (Brewin et al., 2012).

5. Conclusion

In this study, we used a long time series of satellite products to present physical driving forces controlling the phytoplankton biomass and size structure variations, at seasonal and decadal scales, in the BS and YS. Based on a large in situ data set of pigment concentrations from 2014 to 2016, we reparametrized the SST-dependent three-component model in the BS and YS region. By introducing dependence of model parameters on SST, the model captured the variability in size-fractionated chlorophyll-a concentrations better, and had higher accuracy, with lower RMSE, ranging between 0.897, 0.180, and 0.039 mg/m^3 on concentrations and 11.05%, 10.87%, and 2.89% on percentages for microplankton, nanoplankton, and picoplankton, respectively.

Different spatial and temporal distributions of total and size-fractionated chlorophyll-a were observed between coastal and central areas using 20 years of satellite data. The BS and coastal YS showed similar monthly variation, with higher chlorophyll-a concentration from December to March and a dominance of microplankton and nanoplankton throughout the year. A peak of chlorophyll-a concentration was

observed in July in the Changjiang estuary region, and high percentages of microplankton were sustained all year around. The central surface SYS showed higher chlorophyll-a concentrations and microplankton dominance in April, as a result of the increase of solar radiation and the intrusion of Yellow Sea Warm Current since last winter. Meanwhile, from May to October, much lower chlorophyll-a concentrations were observed in the surface central SYS, with a change from microplankton to nanoplankton dominance and a higher contribution from picoplankton, which was due to the existence of YSCWM in the bottom layer. These observations indicated that interactions among solar radiation, circulations, and monsoon winds result in variations in SST, SLA, and MLD, and consequently nutrient concentrations, impacting the spatial and temporal distributions of chlorophyll-a and PSCs.

The 20-year satellite-derived interannual anomalies of chlorophyll-a concentration, PSCs, and SST, in combination with climate indices, indicated that physical and biological responses to each type of El Niño were different in the central SYS. Warmer (colder) SST anomaly during EP El Niño (CP El Niño) events caused lower (higher) chlorophyll-a concentration and microplankton percentage, and higher (lower) nanoplankton and picoplankton percentages in the central SYS. The results highlight that continuous in situ observations and satellite monitoring of physical-biological interactions are required to improve our understanding of ecological and biogeochemical processes under climate change.

Acknowledgments
This work is supported by NSFC project (41771378) and WLKXJ2019-006. The authors thank the European Space Agency for providing Ocean Colour Climate Change Initiative data set, Version 3.1, available online at http://www.esa-oceancolour-cci.org/; the Copernicus Marine Environment Monitoring Service for providing sea level anomaly and mixed layer depth data, available online at http://marine.copernicus.eu/; and Remote Sensing Systems for providing Cross-Calibrated Multi-Platform winds data, available online at http://www.remss.com/measurements/ccmp/. In situ water sample data in the Bohai Sea and Yellow Sea from 2014 to 2016 were obtained from the "Dongfanghong 2" research cruises and all the scientists and crew who participated in the field surveys are sincerely appreciated. We are grateful to the Jingjing Zhang from Ludong University for HPLC pigments data in 2014 and 2015, and Richard G.J. Bellerby group from State Key Laboratory of Estuarine and Coastal Research for HPLC pigments data in 2016 (Projects SKLEC-2016RCDW01 and 13904-41211D-18009). Xuerong Sun is grateful to the China Scholarship Council for supporting a joint PhD study at Plymouth Marine Laboratory. We thank three reviewers for their constructive comments and suggestions. Data results of Figures and Tables in this study is publicly available at https://figshare.com/s/1f84cce2ff5ed3b5340a.

References

Agawin, N. S. R., Duarte, C. M., & Agustí, S. (2000). Nutrient and temperature control of the contribution of picoplankton to phytoplankton biomass and production. *Limnology and Oceanography*, *45*(3), 591–600. https://doi.org/10.4319/lo.2000.45.3.0591

Bai, J., Jiang, Y., Sun, J., & He, Q. (2007). The diurnal fluctuation of phytoplankton vertical distribution adjacent to the Yellow Sea cold water mass. *Periodical of Ocean University of China*, *37*(6), 1013–1016. http://doi.org/10.3969/j.issn.1672-5174.2007.06.016

Behrenfeld, M. J., O'Malley, R. T., Siegel, D. A., McClain, C. R., Sarmiento, J. L., Feldman, G. C., et al. (2006). Climate-driven trends in contemporary ocean productivity. *Nature*, *444*(7120), 752–755. http://doi.org/10.1038/nature05317

Boyce, D. G., Lewis, M. R., & Worm, B. (2010). Global phytoplankton decline over the past century. *Nature*, *466*(7306), 591–596. http://doi.org/10.1038/nature09268

Brewin, R. J. W., Ciavatta, S., Sathyendranath, S., Jackson, T., Tilstone, G., Curran, K., et al. (2017). Uncertainty in ocean-color estimates of chlorophyll for phytoplankton groups. *Frontiers in Marine Science*, *4*, 104. https://doi.org/10.3389/fmars.2017.00104

Brewin, R. J. W., Dall'Olmo, G., Pardo, S., van Dongen-Vogels, V., & Boss, E. S. (2016). Underway spectrophotometry along the Atlantic Meridional Transect reveals high performance in satellite chlorophyll retrievals. *Remote Sensing of Environment*, *183*, 82–97. http://doi.org/10.1016/j.rse.2016.05.005

Brewin, R. J. W., Hardman-Mountford, N. J., Lavender, S. J., Raitsos, D. E., Hirata, T., Uitz, J., et al. (2011). An intercomparison of bio-optical techniques for detecting dominant phytoplankton size class from satellite remote sensing. *Remote Sensing of Environment*, *115*(2), 325–339. http://doi.org/10.1016/j.rse.2010.09.004

Brewin, R. J. W., Hirata, T., Hardman-Mountford, N. J., Lavender, S. J., Sathyendranath, S., & Barlow, R. (2012). The influence of the Indian Ocean Dipole on interannual variations in phytoplankton size structure as revealed by Earth Observation. *Deep-Sea Research Part Ii-Topical Studies in Oceanography*, *77-80*, 117–127. http://doi.org/10.1016/j.dsr2.2012.04.009

Brewin, R. J. W., Sathyendranath, S., Hirata, T., Lavender, S. J., Barciela, R. M., & Hardman-Mountford, N. J. (2010). A three-component model of phytoplankton size class for the Atlantic Ocean. *Ecological Modelling*, *221*(11), 1472–1483. http://doi.org/10.1016/j.ecolmodel.2010.02.014

Brewin, R. J. W., Sathyendranath, S., Jackson, T., Barlow, R., Brotas, V., Airs, R., & Lamont, T. (2015). Influence of light in the mixed-layer on the parameters of a three-component model of phytoplankton size class. *Remote Sensing of Environment*, *168*, 437–450. http://doi.org/10.1016/j.rse.2015.07.004

Bricaud, A., Ciotti, A. M., & Gentili, B. (2012). Spatial-temporal variations in phytoplankton size and colored detrital matter absorption at global and regional scales, as derived from twelve years of SeaWiFS data (1998-2009). *Global Biogeochemical Cycles*, *26*, n/a. http://doi.org/10.1029/2010GB003952

Brotas, V., Brewin, R. J. W., Sá, C., Brito, A. C., Silva, A., Mendes, C. R., et al. (2013). Deriving phytoplankton size classes from satellite data: Validation along a trophic gradient in the eastern Atlantic Ocean. *Remote Sensing of Environment*, *134*, 66–77. http://doi.org/10.1016/j.rse.2013.02.013

Cai, R., Zhang, J., & Qi, Q. (2015). A study on the roIe of East Asian monsoon in variations of sea surface height in the East China Sea and its adjacent seas. *Journal of Applied Oceanography*, *34*(2), 151–158. http://doi.org/10. 3969 /J. ISSN. 2095-4972. 2015. 02. 001

Chakraborty, S., & Lohrenz, S. E. (2015). Phytoplankton community structure in the river-influenced continental margin of the northern Gulf of Mexico. *Marine Ecology Progress Series*, *521*, 31–47. http://doi.org/10.3354/meps11107

Chen, C. T. A. (2009). Chemical and physical fronts in the Bohai, Yellow and East China seas. *Journal of Marine Systems*, *78*(3), 394–410. http://doi.org/10.1016/j.jmarsys.2008.11.016

Ciotti, A. M., & Bricaud, A. (2006). Retrievals of a size parameter for phytoplankton and spectral light absorption by colored detrital matter from water-leaving radiances at SeaWiFS channels in a continental shelf region off Brazil. *Limnology and Oceanography-Methods*, *4*(7), 237–253. http://doi.org/10.4319/lom.2006.4.237

Ciotti, A. M., Lewis, M. R., & Cullen, J. J. (2002). Assessment of the relationships between dominant cell size in natural phytoplankton communities and the spectral shape of the absorption coefficient. *Limnology and Oceanography*, *47*(2), 404–417. http://doi.org/10.4319/lo.2002.47.2.0404

Corredor-Acosta, A., Morales, C., Brewin, R., Auger, P. A., Pizarro, O., Hormazabal, S., & Anabalón, V. (2018). Phytoplankton size structure in association with mesoscale eddies off central-southern Chile: The satellite application of a phytoplankton size-class model. *Remote Sensing*, *10*(6), 834. http://doi.org/10.3390/rs10060834

Cui, T., Zhang, J., Groom, S., Sun, L., Smyth, T., & Sathyendranath, S. (2010). Validation of MERIS ocean-color products in the Bohai Sea: A case study for turbid coastal waters. *Remote Sensing of Environment*, *114*(10), 2326–2336. http://doi.org/10.1016/j.rse.2010.05.009

Devred, E., Sathyendranath, S., Stuart, V., Maass, H., Ulloa, O., & Platt, T. (2006). A two-component model of phytoplankton absorption in the open ocean: Theory and applications. *Journal of Geophysical Research*, *111*, C03011. http://doi.org/10.1029/2005JC002880

Doney, S. C. (2006). Plankton in a warmer world. *Nature*, *444*(7120), 695–696. http://doi.org/10.1038/444695a

Feng, M., Hu, D., & Li, Y. (1992). A theoretical solution for the thermohaline circulation in the Southern Yellow Sea. *Chinese Journal of Oceanology and Limnology*, *10*(4), 289–300. http://doi.org/10.1007/BF02843829

Field, C. B., Behrenfeld, M. J., Randerson, J. T., & Falkowski, P. (1998). Primary Production of the Biosphere: Integrating Terrestrial and Oceanic Components. *Science*, *281*(5374), 237–240. http://doi.org/10.1126/science.281.5374.237

Finkel, Z. V., Beardall, J., Flynn, K. J., Quigg, A., Rees, T. A. V., & Raven, J. A. (2009). Phytoplankton in a changing world: Cell size and elemental stoichiometry. *Journal of Plankton Research*, *32*(1), 119–137. http://doi.org/10.1093/plankt/fbp098

Friedland, K. D., Mouw, C. B., Asch, R. G., Ferreira, A. S. A., Henson, S., Hyde, K. J. W., et al. (2018). Phenology and time series trends of the dominant seasonal phytoplankton bloom across global scales. *Global Ecology and Biogeography*, *27*(5), 551–569. http://doi.org/10.1111/geb.12717

Fu, M., Sun, P., Wang, Z., Li, Y., & Li, R. (2010). Seasonal variations of phytoplankton community size structures in the Huanghai (Yellow) Sea Cold Water Mass area. *Acta Oceanologica Sinica*, *31*(2), 120–129. http://doi.org/10.1515/JOC.2010.31.2.75

Fu, M., Sun, P., Wang, Z., Wei, Q., Qu, P., Zhang, X., & Li, Y. (2018). Structure, characteristics and possible formation mechanisms of the subsurface chlorophyll maximum in the Yellow Sea Cold Water Mass. *Continental Shelf Research*, *165*, 93–105. http://doi.org/10.1016/j.csr.2018.07.007

Fu, M., Wang, Z., Li, Y., Li, R., Sun, P., Wei, X., et al. (2009). Phytoplankton biomass size structure and its regulation in the Southern Yellow Sea (China): Seasonal variability. *Continental Shelf Research*, *29*(18), 2178–2194. http://doi.org/10.1016/j.csr.2009.08.010

Fu, M., Wang, Z., Pu, X., Qu, P., Li, Y., Wei, Q., & Jiang, M. (2016). Response of phytoplankton community to nutrient enrichment in the subsurface chlorophyll maximum in Yellow Sea Cold Water Mass. *Acta Ecologica Sinica*, *36*(1), 39–44. http://doi.org/10.1016/j.chnaes.2015.09.007

Gao, S., & Li, Z. (2009). Spatial and seasonal variation of chlorophyll and primary productivity in summer and winter in the northern Yellow Sea. *Periodical of Ocean University of China*, *39*(4), 604–610. http://doi.org/10.16441/j.cnki.hdxb.2009.04.009

Gierach, M. M., Lee, T., Turk, D., & McPhaden, M. J. (2012). Biological response to the 1997–98 and 2009–10 El Niño events in the equatorial Pacific Ocean. *Geophysical Research Letters*, *39*, L10602. https://doi.org/10.1029/2012GL051103

Gittings, J. A., Raitsos, D. E., Racault, M. F., Brewin, R. J. W., Pradhan, Y., Sathyendranath, S., & Platt, T. (2017). Seasonal phytoplankton blooms in the Gulf of Aden revealed by remote sensing. *Remote Sensing of Environment*, *189*, 56–66. http://doi.org/10.1016/j.rse.2016.10.043

Gomes, H. D. R., Xu, Q., Ishizaka, J., Carpenter, E. J., Yager, P. L., & Goes, J. I. (2018). The influence of riverine nutrients in niche partitioning of phytoplankton communities–A contrast between the Amazon River Plume and the Changjiang (Yangtze) River diluted water of the East China Sea. *Frontiers in Marine Science*, *5*, 343. http://doi.org/10.3389/fmars.2018.00343

González Taboada, F., & Anadón, R. (2014). Seasonality of North Atlantic phytoplankton from space: Impact of environmental forcing on a changing phenology (1998-2012). *Global Change Biology*, *20*(3), 698–712. http://doi.org/10.1111/gcb.12352

Gregg, W. W., & Conkright, M. E. (2002). Decadal changes in global ocean chlorophyll. *Geophysical Research Letters*, *29*, 20-1–20-4. http://doi.org/10.1029/2002GL014689

Guidi, L., Stemmann, L., Jackson, G. A., Ibanez, F., Claustre, H., Legendre, L., et al. (2009). Effects of phytoplankton community on production, size and export of large aggregates: A world-ocean analysis. *Limnology and Oceanography*, *54*(6), 1951–1963. http://doi.org/10.4319/lo.2009.54.6.1951

He, C., Wang, Y., Lei, Z., & Xu, S. (1959). A preliminary study of the formation of Yellow Sea cold mass and its properties. *Oceanologia Et Limnologia Sinica*, *2*(1), 11–15.

He, X., Bai, Y., Pan, D., Chen, C. T. A., Cheng, Q., Wang, D., & Gong, F. (2013). Satellite views of the seasonal and interannual variability of phytoplankton blooms in the eastern China seas over the past 14 yr (1998-2011). *Biogeosciences*, *10*(7), 4721–4739. http://doi.org/10.5194/bg-10-4721-2013

Hirata, T., Hardman-Mountford, N. J., Brewin, R. J. W., Aiken, J., Barlow, R., Suzuki, K., et al. (2011). Synoptic relationships between surface Chlorophyll-a and diagnostic pigments specific to phytoplankton functional types. *Biogeosciences*, *8*(2), 311–327. http://doi.org/10.5194/bg-8-311-2011

Huang, D., Zhang, T., & Zhou, F. (2010). Sea-surface temperature fronts in the Yellow and East China Seas from TRMM microwave imager data. *Deep-Sea Research Part Ii-Topical Studies in Oceanography*, *57*(11-12), 1017–1024. http://doi.org/10.1016/j.dsr2.2010.02.003

Hwang, J. H., Van, S. P., Choi, B. J., Chang, Y. S., & Kim, Y. H. (2014). The physical processes in the Yellow Sea. *Ocean and Coastal Management*, *102*, 449–457. http://doi.org/10.1016/j.ocecoaman.2014.03.026

Hyun, J., & Kim, K. (2003). Bacterial abundance and production during the unique spring phytoplankton bloom in the central Yellow Sea. *Marine Ecology Progress Series*, *252*(1), 77–88. http://doi.org/10.3354/meps252077

IOCCG (2000). Remote sensing of ocean colour in coastal, and other optically-complex, waters. In S. Sathyendranath (Ed.), *Reports of the International Ocean-Colour Coordinating Group, No. 3* (Chap. 2, pp. 23). Dartmouth, Canada: IOCCG.

IOCCG (2014). Phytoplankton functional types from space. In S. Sathyendranath (Ed.), *Reports of the International Ocean-Colour Coordinating Group, No. 15* (Chap. 4, pp. 71). Dartmouth, Canada: IOCCG.

IPCC (2013). Climate Change 2013: The physical science basis. In T. F. Stocker, D. Qin, G.-K. Plattner, M. Tignor, S. K. Allen, J. Boschung, A. Nauels, Y. Xia, V. Bex, & P. M. Midgley (Eds.), *Contribution of Working Group I to the Fifth Assessment Report of the Intergovernmental Panel on Climate Change* (Chap. 12, p. 1033). Cambridge, United Kingdom and New York, NY, USA: Cambridge University Press. http://doi.org/10.1017/CBO9781107415324

Jiang, Z., Chen, J., Gao, Y., Zhai, H., Jin, H., Zhou, F., et al. (2019). Regulation of spatial changes in phytoplankton community by water column stability and nutrients in the southern Yellow Sea. *Journal of Geophysical Research: Biogeosciences*, *124*(8), 2610–2627. http://doi.org/10.1029/2018JG004785

Jiang, Z., Liu, J., Chen, J., Chen, Q., Yan, X., Xuan, J., & Zeng, J. (2014). Responses of summer phytoplankton community to drastic environmental changes in the Changjiang (Yangtze River) estuary during the past 50 years. *Water Research*, *54*, 1–11. http://doi.org/10.1016/j.watres.2014.01.032

Jin, J., Liu, S. M., Ren, J. L., Liu, C. G., Zhang, J., Zhang, G. L., & Huang, D. J. (2013). Nutrient dynamics and coupling with phytoplankton species composition during the spring blooms in the Yellow Sea. *Deep Sea Research Part II: Topical Studies in Oceanography*, *97*(12), 16–32. http://doi.org/10.1016/j.dsr2.2013.05.002

Kao, H. Y., & Yu, J. Y. (2009). Contrasting eastern-pacific and central-pacific types of ENSO. *Journal of Climate*, *22*(3), 615–632. http://doi.org/10.1175/2008JCLI2309.1

Kostadinov, T. S., Siegel, D. A., & Maritorena, S. (2009). Retrieval of the particle size distribution from satellite ocean color observations. *Journal of Geophysical Research*, *114*, C09015. http://doi.org/10.1029/2009JC005303

Kostadinov, T. S., Siegel, D. A., & Maritorena, S. (2010). Global variability of phytoplankton functional types from space: Assessment via the particle size distribution. *Biogeosciences*, *7*(10), 3239–3257. http://doi.org/10.5194/bg-7-3239-2010

Lamont, T., Brewin, R. J. W., & Barlow, R. G. (2018). Seasonal variation in remotely-sensed phytoplankton size structure around southern Africa. *Remote Sensing of Environment*, *204*, 617–631. http://doi.org/10.1016/j.rse.2017.09.038

Li, G., Qiao, L., Dong, P., Ma, Y., Xu, J., Liu, S., et al. (2016). Hydrodynamic condition and suspended sediment diffusion in the Yellow Sea and East China Sea. *Journal of Geophysical Research: Oceans*, *121*, 6204–6222. http://doi.org/10.1002/2015JC011442

Lin, X., Yang, J., Guo, J., Zhang, Z., Yin, Y., Song, X., & Zhang, X. (2011). An asymmetric upwind flow, Yellow Sea Warm Current: 1. New observations in the western Yellow Se. *Journal of Geophysical Research*, *116*, C04026. http://doi.org/10.1029/2010JC006513

Liu, D., & Wang, Y. (2013). Trends of satellite derived chlorophyll-a (1997–2011) in the Bohai and Yellow Seas, China: Effects of bathymetry on seasonal and inter-annual patterns. *Progress in Oceanography*, *116*, 154–166. http://doi.org/10.1016/j.pocean.2013.07.003

Liu, X., Huang, B., Huang, Q., Wang, L., Ni, X., Tang, Q., et al. (2015). Seasonal phytoplankton response to physical processes in the southern Yellow Sea. *Journal of Sea Research*, *95*, 45–55. http://doi.org/10.1016/j.seares.2014.10.017

Liu, X., Huang, B., Liu, Z., Wang, L., Wei, H., Li, C., & Huang, Q. (2012). High-resolution phytoplankton diel variations in the summer stratified central Yellow Sea. *Journal of Oceanography*, *68*(6), 913–927. http://doi.org/10.1007/s10872-012-0144-6

Longhurst, A., Sathyendranath, S., Platt, T., & Caverhill, C. (1995). An estimate of global primary production in the ocean from satellite radiometer data. *Journal of Plankton Research*, *17*(6), 1245–1271. http://doi.org/10.1093/plankt/17.6.1245

McClain, C. R. (2009). A decade of satellite ocean color observations. *Annual Review of Marine Science*, *1*(1), 19–42. http://doi.org/10.1146/annurev.marine.010908.163650

Mélin, F. (2016). Impact of inter-mission differences and drifts on chlorophyll-a trend estimates. *International Journal of Remote Sensing*, *37*(10), 2233–2251. http://doi.org/10.1080/01431161.2016.1168949

Mélin, F., Vantrepotte, V., Chuprin, A., Grant, M., Jackson, T., & Sathyendranath, S. (2017). Assessing the fitness-for-purpose of satellite multi-mission ocean color climate data records: A protocol applied to OC-CCI chlorophyll- a data. *Remote Sensing of Environment*, *203*, 139–151. http://doi.org/10.1016/j.rse.2017.03.039

Mouw, C. B., Ciochetto, A. B., & Yoder, J. A. (2019). A satellite assessment of environmental controls of phytoplankton community size structure. *Global Biogeochemical Cycles*, *33*(5), 540, 2018GB006118–558. http://doi.org/10.1029/2018GB006118

Mouw, C. B., Hardman-Mountford, N. J., Alvain, S., Bracher, A., Brewin, R. J. W., Bricaud, A., et al. (2017). A consumer's guide to satellite remote sensing of multiple phytoplankton groups in the global ocean. *Frontiers in Marine Science*, *4*(41). http://doi.org/10.3389/fmars.2017.00041

Nair, A., Sathyendranath, S., Platt, T., Morales, J., Stuart, V., Forget, M., et al. (2008). Remote sensing of phytoplankton functional types. *Remote Sensing of Environment*, *112*(8), 3366–3375. http://doi.org/10.1016/j.rse.2008.01.021

Oh, K. H., Lee, S., Song, K. M., Lie, H. J., & Kim, Y. T. (2013). The temporal and spatial variability of the Yellow Sea Cold Water Mass in the southeastern Yellow Sea, 2009–2011. *Acta Oceanologica Sinica*, *32*(9), 1–10. http://doi.org/10.1007/s13131-013-0346-9

Paek, H., Yu, J., & Qian, C. (2017). Why were the 2015/2016 and 1997/1998 extreme El Niños different? *Geophysical Research Letters*, *44*, 1848–1856. http://doi.org/10.1002/2016GL071515

Park, S., Chu, P. C., & Lee, J. (2011). Interannual-to-interdecadal variability of the Yellow Sea Cold Water Mass in 1967–2008: Characteristics and seasonal forcings. *Journal of Marine Systems*, *87*(3-4), 177–193. http://doi.org/10.1016/j.jmarsys.2011.03.012

Qiao, X. (2005). *Satellite altimeter based sea level analysis of China seas for the period 1992-2004, Master thesis* (p. 61). Qingdao, China: Ocean University of China.

Racault, M., Raitsos, D. E., Berumen, M. L., Brewin, R. J. W., Platt, T., Sathyendranath, S., & Hoteit, I. (2015). Phytoplankton phenology indices in coral reef ecosystems: Application to ocean-color observations in the Red Sea. *Remote Sensing of Environment*, *160*, 222–234. http://doi.org/10.1016/j.rse.2015.01.019

Racault, M., Sathyendranath, S., Brewin, R. J. W., Raitsos, D. E., Jackson, T., & Platt, T. (2017). Impact of El Niño variability on oceanic phytoplankton. *Frontiers in Marine Science*, *4*, 133. http://doi.org/10.3389/fmars.2017.00133

Raitsos, D. E., Lavender, S. J., Maravelias, C. D., Haralabous, J., Richardson, A. J., & Reid, P. C. (2008). Identifying four phytoplankton functional types from space: An ecological approach. *Limnology and Oceanography*, *53*(2), 605–613. http://doi.org/10.4319/lo.2008.53.2.0605

Reynolds, C. S., Huszar, V., Kruk, C., Naselli-Flores, L., & Melo, S. (2002). Towards a functional classification of the freshwater phytoplankton. *Journal of Plankton Research*, *24*(5), 417–428. http://doi.org/10.1093/plankt/24.5.417

Sathyendranath, S., Brewin, R. J. W., Jackson, T., Mélin, F., & Platt, T. (2017). Ocean-colour products for climate-change studies: What are their ideal characteristics? *Remote Sensing of Environment*, *203*, 125–138. http://doi.org/10.1016/j.rse.2017.04.017

Sathyendranath, S., Cota, G., Stuart, V., Maass, H., & Platt, T. (2001). Remote sensing of phytoplankton pigments: A comparison of empirical and theoretical approaches. *International Journal of Remote Sensing*, *22*(2-3), 249–273. http://doi.org/10.1080/014311601449925

Shi, W., & Wang, M. (2012). Satellite views of the Bohai Sea, Yellow Sea, and East China Sea. *Progress in Oceanography*, *104*, 30–45. http://doi.org/10.1016/j.pocean.2012.05.001

Sieburth, J. M., Smetacek, V., & Lenz, J. (1978). Pelagic ecosystem structure: Heterotrophic compartments of the plankton and their relationship to plankton size fractions. *Limnology and Oceanography*, *23*(6), 1256–1263. https://doi.org/10.4319/lo.1978.23.6.1256

Sin, Y., Wetzel, R. L., & Anderson, I. C. (2000). Seasonal variations of size-fractionated phytoplankton along the salinity gradient in the York River estuary, Virginia (USA). *Journal of Plankton Research*, *22*(10), 1945–1960. http://doi.org/10.1093/plankt/22.10.1945

Sun, D., Huan, Y., Qiu, Z., Hu, C., Wang, S., & He, Y. (2017). Remote-sensing estimation of phytoplankton size classes from GOCI satellite measurements in Bohai Sea and Yellow Sea. *Journal of Geophysical Research: Oceans*, *122*, 8309–8325. http://doi.org/10.1002/2017JC013099

Sun, D., Huan, Y., Wang, S., Qiu, Z., Ling, Z., Mao, Z., & He, Y. (2019). Remote sensing of spatial and temporal patterns of phytoplankton assemblages in the Bohai Sea, Yellow Sea, and east China sea. *Water Research*, *157*, 119–133. http://doi.org/10.1016/j.watres.2019.03.081

Sun, J., Liu, D., Yang, S., Guo, J., & Qian, S. (2002). The preliminary study on phytoplankton community structure in the central Bohai sea and the Bohai strait and its adjacent area. *Oceanologia Et Limnologia Sinica*, *33*(5), 461–471.

Sun, X., Shen, F., Liu, D., Bellerby, R. G. J., Liu, Y., & Tang, R. (2018). In situ and satellite observations of phytoplankton size classes in the entire continental shelf sea, China. *Journal of Geophysical Research: Oceans*, *123*(5), 3523–3544. http://doi.org/10.1029/2017JC013651

Sun, X. X., Ren, L. L., Zheng, S., Wen, F., Zhao, Y. F., & Sun, S. (2012). Phytoplankton size structure in the yellow sea and East China Sea in the spring and summer of 2011. *Oceanologia Et Limnologia Sinica*, *43*, 419–428.

Takahashi, K., Montecinos, A., Goubanova, K., & Dewitte, B. (2011). ENSO regimes: Reinterpreting the canonical and Modoki El Niño. *Geophysical Research Letters*, *38*, L10704. http://doi.org/10.1029/2011GL047364

Tang, Y. X., Zou, E., Lie, H. J., & Lie, J. H. (2000). Some features of circulation in the southern Huanghai Sea. *Acta Oceanologica Sinica*, *22*(1), 1–16. http://doi.org/10.3321/j.issn:0253-4193.2000.01.001

Uitz, J., Claustre, H., Morel, A., & Hooker, S. B. (2006). Vertical distribution of phytoplankton communities in open ocean: An assessment based on surface chlorophyll. *Journal of Geophysical Research*, *111*, C08005. http://doi.org/10.1029/2005JC003207

Uitz, J. U., Huot, Y., Bruyant, F., Babin, M., & Claustre, H. (2008). Relating phytoplankton photophysiological properties to community structure on large scale. *Limnology and Oceanography*, *53*(2), 614–630. http://doi.org/10.4319/lo.2008.53.2.0614

Vidussi, F., Claustre, H., Manca, B. B., Luchetta, A., & Marty, J. C. (2001). Phytoplankton pigment distribution in relation to upper thermocline circulation in the eastern Mediterranean Sea during winter. *Journal of Geophysical Research*, *106*(C9), 19,939–19,956. http://doi.org/10.1029/1999JC000308

Wang, B., Wang, X., & Zhan, R. (2003). Nutrient conditions in the Yellow Sea and the East China Sea. *Estuarine Coastal and Shelf Science*, *58*(1), 127–136. http://doi.org/10.1016/S0272-7714(03)00067-2

Wang, D., Huang, B., Liu, X., Liu,G., & Wang, H. (2014). Seasonal variations of phytoplankton phosphorus stress in the Yellow Sea Cold Water Mass. *Acta Oceanologica Sinica*, *33*(10), 124–135. https://doi.org/10.1007/s13131-014-0547-x

Wang, L., Huang, B., Chiang, K., Liu, X., Chen, B., Xie, Y., et al. (2016). Physical-biological coupling in the western South China Sea: The response of phytoplankton community to a mesoscale cyclonic eddy. *Plos One*, *11*(4), e0153735. http://doi.org/10.1371/journal.pone.0153735

Wang, Z., Zuo, J., Chen, M., Xu, Q., & Yang, Y. (2012). Relationship between El Nino and sea surface temperature variation in coastal region of Yellow Sea and East China Sea. *Journal of Hohai University: Natural Sciences*, *40*(4), 461–468. http://doi.org/10.3876/j.issn.1000-1980.2012.04.018

Ward, B. A. (2015). Temperature-correlated changes in phytoplankton community structure are restricted to polar waters. *Plos One*, *10*(8), e0135581. http://doi.org/10.1371/journal.pone.0135581

Ward, B. A., Dutkiewicz, S., Jahn, O., & Follows, M. J. (2012). A size-structured food-web model for the global ocean. *Limnology and Oceanography*, *57*(6), 1877–1891. http://doi.org/10.4319/lo.2012.57.6.1877

Wei, J., Lee, Z., & Shang, S. (2016). A system to measure the data quality of spectral remote-sensing reflectance of aquatic environments. *Journal of Geophysical Research: Oceans*, *121*, 8189–8207. http://doi.org/10.1002/2016JC012126

Wei, Q., Yu, Z., Wang, B., Fu, M., Xia, C., Liu, L., et al. (2016). Coupling of the spatial–temporal distributions of nutrients and physical conditions in the southern Yellow Sea. *Journal of Marine Systems*, *156*, 30–45. http://doi.org/10.1016/j.jmarsys.2015.12.001

Xin, M., Ma, D., & Wang, B. (2015). Chemicohydrographic characteristics of the Yellow Sea Cold Water Mass. *Acta Oceanologica Sinica*, *34*(6), 5–11. https://doi.org/10.1007/s13131-015-0681-0

Xu, Q., Sukigara, C., Goes, J. I., Do Rosario Gomes, H., Zhu, Y., Wang, S., et al. (2019). Interannual changes in summer phytoplankton community composition in relation to water mass variability in the East China Sea. *Journal of Oceanography*, *75*(1), 61–79. http://doi.org/10.1007/s10872-018-0484-y

Xuan, J., Zhou, F., Huang, D., Wei, H., Liu, C., & Xing, C. (2011). Physical processes and their role on the spatial and temporal variability of the spring phytoplankton bloom in the central Yellow Sea. *Acta Ecologica Sinica*, *31*(1), 61–70. http://doi.org/10.1016/j.chnaes.2010.11.011

Yamaguchi, H., Ishizaka, J., Siswanto, E., Baek Son, Y., Yoo, S., & Kiyomoto, Y. (2013). Seasonal and spring interannual variations in satellite-observed chlorophyll-a in the Yellow and East China Seas: New datasets with reduced interference from high concentration of resuspended sediment. *Continental Shelf Research*, *59*, 1–9. http://doi.org/10.1016/j.csr.2013.03.009

Yu, F., Zhang, Z., Diao, X., Guo, J., & Tang, Y. (2006). Analysis of evolution of the Huanghai Sea Cold Water Mass and its relationship with adjacent water masses. *Acta Oceanologica Sinica*, *17*(2), 106–112. http://doi.org/10.1016/S1001-8042(06)60021-3

Yu, J., & Kim, S. T. (2013). Identifying the types of major El Niño events since 1870. *International Journal of Climatology*, *33*(8), 2105–2112. http://doi.org/10.1002/joc.3575

Yu, Z., Mi, T., Xie, B., Yao, Q., & Zhang, J. (2000). Changes of the environmental parameters and their relationship in recent twenty years in the Bohai Sea. *Marine Environmental Science*, *19*(1), 15–19.

Yuan, Y., & Yang, S. (2012). Impacts of different types of El Niño on the East Asian climate: Focus on ENSO cycles. *Journal of Climate*, *25*(21), 7702–7722. http://doi.org/10.1175/JCLI-D-11-00576.1

Zhang, J., Liu, D., Cao, P., Wang, Y., Keesing, J. K., Li, J., & Chen, L. (2016). A highly sensitive method for analyzing marker phytoplankton pigments: Ultra-high-performance liquid chromatography-tandem triple quadrupole mass spectrometry. *Limnology and Oceanography: Methods*, *14*(10), 623–636. http://doi.org/10.1002/lom3.10117

Zhang, S. W., Wang, Q. Y., Lü, Y., Cui, H., & Yuan, Y. L. (2008). Observation of the seasonal evolution of the Yellow Sea Cold Water Mass in 1996–1998. *Continental Shelf Research*, *28*(3), 442–457. http://doi.org/10.1016/j.csr.2007.10.002

Zhou, M., Shen, Z., & Yu, R. (2008). Responses of a coastal phytoplankton community to increased nutrient input from the Changjiang (Yangtze) River. *Continental Shelf Research*, *28*(12), 1483–1489. http://doi.org/10.1016/j.csr.2007.02.009

Zhu, J., Shi, J., Guo, X., Gao, H., & Yao, X. (2018). Air-sea heat flux control on the Yellow Sea Cold Water Mass intensity and implications for its prediction. *Continental Shelf Research*, *152*, 14–26. http://doi.org/10.1016/j.csr.2017.10.006

Zhu, Z., Ng, W., Liu, S., Zhang, J., Chen, J., & Wu, Y. (2009). Estuarine phytoplankton dynamics and shift of limiting factors: A study in the Changjiang (Yangtze River) Estuary and adjacent area. *Estuarine, Coastal and Shelf Science*, *84*(3), 393–401. http://doi.org/10.1016/j.ecss.2009.07.005